Ignatov et al., 2003b). HA had no effect on GPR99, GPR100, GalRL, GPR1, GPR7, GPR8, GPR19, GPR75 and SALPR, just to name a few. Of special interest was a sub-branch of GPCRs that regulate cellular proliferation, namely the endothelin, bombesin and neuromedin receptors. Two orphan receptors are part of this group: GPR37 and GPR37L1 (Marazziti et al., 2001). We focused our interest on GPR37 because of its prominent expression in neurons of the brain compared with a more glial location of GPR37L1 (Marazziti et al., 1997; Zeng et al., 1997). GPR37 has also been isolated and characterised as a substrate for the ubiquitin ligase parkin, hence its alternative name – parkin-associated endothelin-like receptor (Pael R) (Imai et al., 2001). GPR37 was shown to fold improperly in the absence of parkin, and its aggregation to insoluble complexes results in endoplasmic reticulum stress (Imai et al., 2001; Imai et al., 2003). This leads to preferential loss of dopaminergic neurons in the substantia nigra and contributes to neurodegeneration in Parkinson's disease (Yang et al., 2003). Accumulation of GPR37 in Lewy bodies in the brain of patients with Parkinson's disease supports this notion (Murakami et al., 2004).

To study a possible interaction of HA with GPR37, various assay systems were used that allow detection, directly or indirectly, of ligand-receptor interactions. In this paper, we present evidence that HA is a high-affinity ligand for GPR37.

Results

HA stimulates internalisation of GPR37 in COS-7 cells

We tried to express GPR37 heterologously in Chinese hamster ovary (CHO-K1) cells, in human embryonic kidney (HEK-293) cells and in green monkey kidney (COS-7) cells. Transient transfection efficiencies in HEK-293 and CHO-K1 cells were far below 5%, and cells expressing GPR37 looked sick and decreased in number at 48 hours compared with 24 hours after transfection. Transfection efficiencies in COS-7 cells were better and reached levels in the range of 15-30% (Fig. 1A). COS-7 cells were therefore suitable for experiments with individual, transfected cells. There was no difference in expression levels between GPR37 with (Fig. 1B) and without (Fig. 1C) FLAG tag at the C-terminus. This indicated that the tag did not interfere with GPR37 protein biosynthesis and localisation. GPR37 immunoreactivity was visible in the cytoplasm of transfected COS-7 cells, but also extended to cell protrusions, hinting at cell-surface expression (Fig. 1B,C). Cell-surface expression was confirmed by treating living cells before fixation with a monoclonal antibody against GPR37 (Fig. 1D) that reacts with extracellular epitopes of GPR37 (Imai et al., 2001).

HA treatment of COS-7 cells transiently transfected with GPR37-FLAG led to internalisation of the receptor. This was visible as disappearance of the GPR37-FLAG immunoreactivity from the protrusions after 10 minutes (compare Fig. 1E and F), and as translocation into the cytoplasm after 20 minutes (Fig. 1G). Protrusions started to show FLAG staining again after 30-60 minutes (Fig. 1H,I).

GPR37 aggregation is prevented by stable inducible expression in HEK-293 cells

Transient expression of GPR37 led in all cell lines assayed to aggregation of complexes with apparent molecular masses of ≥250 kDa (Fig. 2A). Surface biotinylation showed that only the monomeric receptor appeared at the outer cell membrane (Fig. 2B), indicating that most of the overproduced GPR37 was not properly folded, stayed in the cytoplasm and was probably

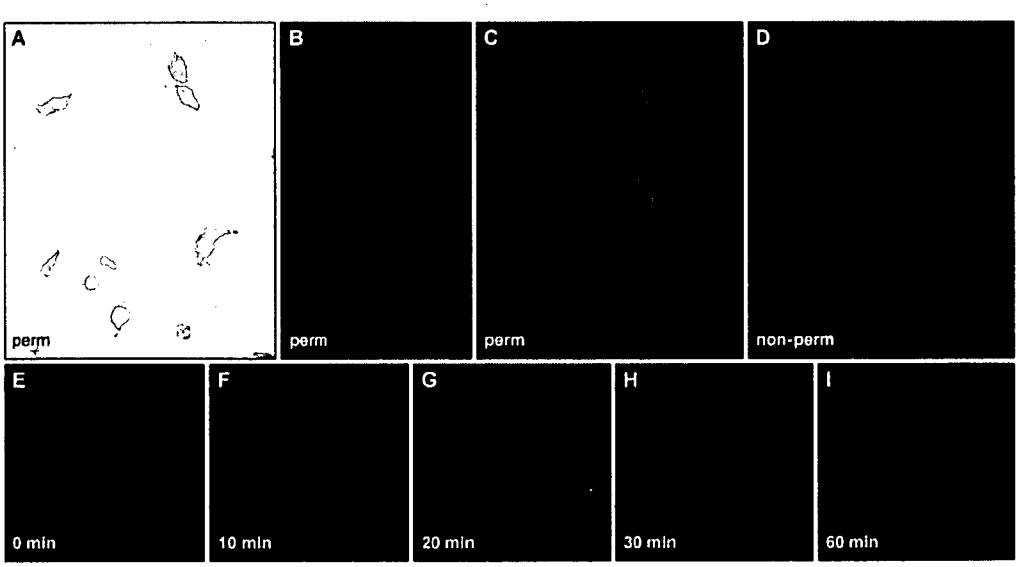

Fig. 1. GPR37 is expressed at the cell surface of COS-7 cells and internalises after HA treatment. (A-I) COS-7 cells were transfected with GPR37 with (B,D-I) or without (A,C) FLAG tag, immunostained with anti-GPR37 antibody (A,C,D) or with anti-FLAG antibody (B,E-I) and visualised with alkaline phosphatase-coupled secondary antibodies for light microscopy (A) or with Cy3-coupled antibodies for confocal analysis (B-I). Cells were permeabilised (perm) by fixation with 1% acetic acid in ethanol and by washing with Triton X-100, except in D, where living cells were incubated with the primary antibody before fixation (non-perm) to show surface staining. (E-I) COS-7 cells 48 hours after transfection with GPR37-FLAG were treated at 37°C with 2 nM HA for 0, 10, 20, 30 and 60 minutes, respectively, and immunostained with anti-FLAG antibody.

degraded (Imai et al., 2001). To prevent aggregation and subsequent degradation, we integrated GPR37 stably into HEK-T-REx cells with a construct that allowed induction by tetracycline (HEK-T-REx–GPR37). Incubation of cells with the tetracycline derivative doxycycline for 24 hours resulted in production predominantly of the monomeric form of GPR37 (Fig. 2C, first lane). Without doxycycline induction, GPR37 was not detectable (Fig. 2C, second lane). Confocal image analysis revealed that, after induction with doxycycline, GPR37 localised mainly to the outer cell membrane, both in permeabilised (Fig. 2D) and non-permeabilised cells (Fig. 2F). The non-induced cells showed no GPR37 immunoreactivity (Fig. 2E,G). To study internalisation, HEK-T-REx–GPR37 cells were incubated in defined medium for 24 hours with doxycycline to induce GPR37 expression. Subsequent treatment with HA for 10 minutes led to rapid internalisation of GPR37 (Fig. 2H,I). This internalisation was much faster in HEK than in COS-7 cells, probably as a result of differences in β-arrestin levels (Ménard et al., 1997).

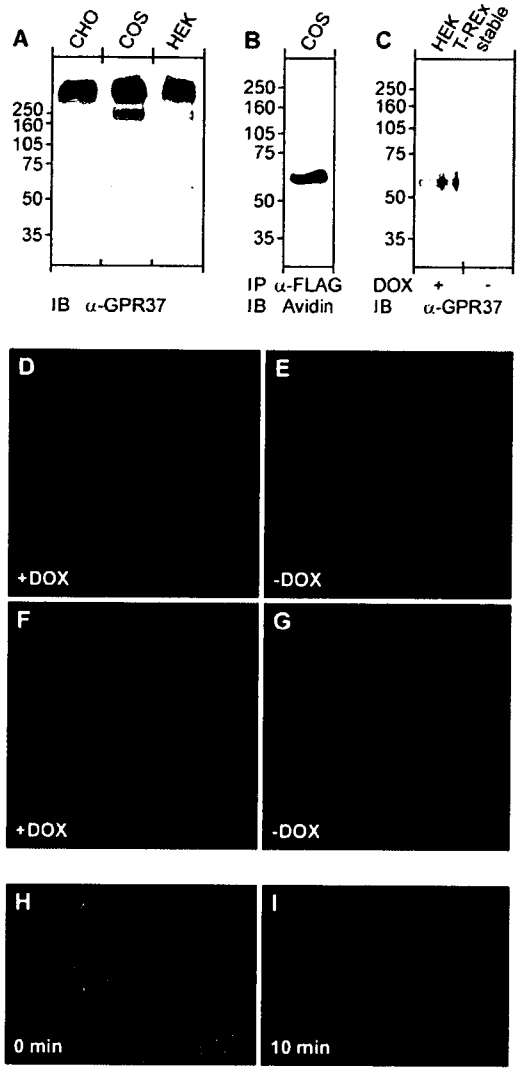

Fig. 2. Inducible, stable expression of GPR37 prevents aggregate formation. (A) CHO-K1, COS-7 and HEK-293 cells were transiently transfected with GPR37, and membrane fractions were assayed by immunoblotting (IB) with anti-GPR37 antibody (α-GPR37). (B) COS-7 cells transiently transfected with GPR37-FLAG were cell-surface biotinylated, and the solubilised membrane fraction was immunoprecipated (IP) with anti-FLAG antibody (α-FLAG) and visualised after immunoblotting with avidin. (C) GPR37 was introduced stably into the flip-in cell line HEK-T-REx, where GPR37 expression is inducible by doxycycline (DOX). Membrane fractions were subjected to western blotting with anti-GPR37 antibody (α-GPR37) with (first lane) and without (second lane) induction for 24 hours with doxycycline. (D-I) HEK-T-REx–GPR37 cells with (D,F,H,I) and without (E,G) doxycycline induction for 24 hours were immunostained with anti-GPR37(R2) antibody after permeabilisation (D,E) and with anti-GPR37 antibody without permeabilisation (F-I). (H,I) HEK-T-REx–GPR37 cells were treated with 2 nM HA for 0 and 10 minutes at 37°C, respectively, fixed with 2% formaldehyde for 10 minutes and subsequently immunostained with anti-GPR37 antibody.

HA binds to GPR37

To show direct interaction of HA with GPR37, COS-7 cells were analysed after incubation with 2 nM HA by fluorescence resonance energy transfer (FRET). Localisation of HA was detected with a HA-specific polyclonal antiserum and was visualised with a Cy2-coupled secondary antibody (green). To detect GPR37, monoclonal antibodies directed against the extracellular domain of human GPR37 were used in combination with a Cy3-coupled secondary antibody (red). Fig. 3A-D shows a typical example of FRET between HA and ectodomains of GPR37. After bleaching a discrete area in a GPR37-positive cell (Fig. 3A,B), an increase in HA fluorescence was observed (Fig. 3C,D). The difference in staining pattern is due to the fact that COS-7 cells, in addition to GPR37, express endogenous HA receptor(s) (Boels et al., 2001). The experiment was repeated several times on different days yielding similar results. On average, the calculated energy-transfer efficiencies were in the range of 19.4±4.5%, indicating the close association of GPR37 and HA. Non-transfected cells were negative, and no transfer of signal was obtained if an antibody against the FLAG tag at the C-terminus of GPR37 was used (data not shown).

For visualisation of HA binding to GPR37, a fluorescent derivative of HA was produced. For this purpose, the fluorophore Cy3B was coupled to the ϵ-amino group of Lys7 of HA. The neuroblastoma cell line NH15-CA2, which reacts with HA (Ulrich et al., 1996) and endogenously expresses GPR37 (Fig. 3E), was used as positive control. Binding of Cy3B-labelled HA to NH15-CA2 cells was observed starting from a concentration of 50 nM, with optimal binding at 150 nM, achieved after incubation for 10 minutes at 37°C (Fig. 3F). Pre-incubation with unlabelled HA for 50 minutes prevented Cy3B-HA binding (Fig. 3G). Cy3B-labelled HA did not bind to HEK-T-REx–GPR37 cells without induction of GPR37 expression by doxycycline (Fig. 3H), but reacted after induction for 24 hours with doxycycline (Fig. 3I). Pre-incubation with unlabelled HA inhibited binding (Fig. 3J), demonstrating that the two ligands compete for the same receptor and that the receptor is either occupied or, more likely, internalised after interaction with HA.

HA induces an increase in Ca^{2+} mobilisation in cells expressing GPR37

To confirm the interaction of HA with GPR37, Ca^{2+} mobilisation was measured in CHO-K1 cells stably

transfected with apoaequorin as Ca^{2+} sensor and with the promiscuous G-protein subunit Gα16 for signal enhancement. After reconstitution with the aequorin cofactor coelenterazine, agonist action was monitored as increase in bioluminescence (Stables et al., 1997). Since GPR37 was not sufficiently expressed in this cell line (CHO) by transient transfection, a stable cell line was established that, in addition to Gα16 and apoaequorin, also expressed GPR37 (CHO-GPR37). Treatment of these cells with HA dose dependently led to an increase in Ca^{2+} mobilisation with an EC_{50} value of 3.3 nM (Fig. 4A). To our surprise, an endogenous response was also observed (Fig. 4A). Northern blots were negative, but immunocytochemistry (Fig. 4B) and western blots (Fig. 4C) probed with an antiserum against the very conserved intracellular C-tail confirmed presence of GPR37 in CHO cells. The hippocampal mouse cell line HT22, expressing GPR37 endogenously, was used as a positive control (Fig. 4C). The active monomeric form of GPR37 was predominantly present both in CHO-GPR37 and HT22 cells.

HA stimulates a current increase in frog oocytes expressing GPR37

In our hands, the frog oocyte system has proven to be very reliable and robust for studying the interaction of ligands with orphan GPCRs (Ignatov et al., 2003a; Ignatov et al., 2003b). Since HA signal transduction for mitotic stimulation is coupled to an inhibitory G protein (Kayser et al., 1998; Ulrich et al., 1996), frog oocytes were injected not only with complementary RNAs (cRNAs) coding for human GPR37, but also with cRNAs coding for the G-protein-coupled inwardly rectifying K^+ channel GIRK, which is activated by βγ subunits of inhibitory G proteins (Kofuji et al., 1995). The concatemer between GIRK1 and GIRK2 (GIRK1/2) was chosen to enhance the current increase and improve the signal to noise ratio (Wischmeyer et al., 1997). Treatment with HA led to an additional increase in the basal inward current induced by changing the external bath medium to high K^+ in oocytes expressing GPR37 together with GIRK1/2 (Fig. 5A). A minute, negligible response was also obtained with medium alone (Fig. 5A). The effect of HA was concentration dependent, and a dose-response curve yielded an EC_{50} value of 5.6 nM (Fig. 5B). Since HA was diluted about twofold by addition to the oocyte bath medium, this EC_{50} value is in agreement with that obtained in the Ca^{2+}-mobilisation assay in CHO cells. Oocytes expressing GIRK1/2 without GPR37 were unresponsive to HA (Fig. 5B). Comparable dose-response curves were obtained from 30 oocytes.

HA signal transduction

One of the most prominent effects of HA is that it stimulates cells to enter mitosis (Hampe et al., 2000; Kayser et al., 1998; Ulrich et al., 1996). At the G2-mitosis transition, histone H3 is phosphorylated and is, therefore, an excellent marker for mitotic events. HEK-T-REx–GPR37 cells were incubated with and without doxycycline for 24 hours, before HA was added for 1.7 hours. Cells induced with doxycycline to express GPR37 showed an increase over uninduced cells in the percentage of mitotic cells, as visualised with the antibody against phosphorylated histone H3 (Fig. 6A). This suggested a direct role for GPR37 in mediating the action of HA as a mitogen. To monitor HA signalling mediated by GPR37, transiently transfected COS-7 cells and HEK-T-REx–GPR37 cells were subjected to electrophysiological analysis by patch clamping. Treatment of cells with HA led

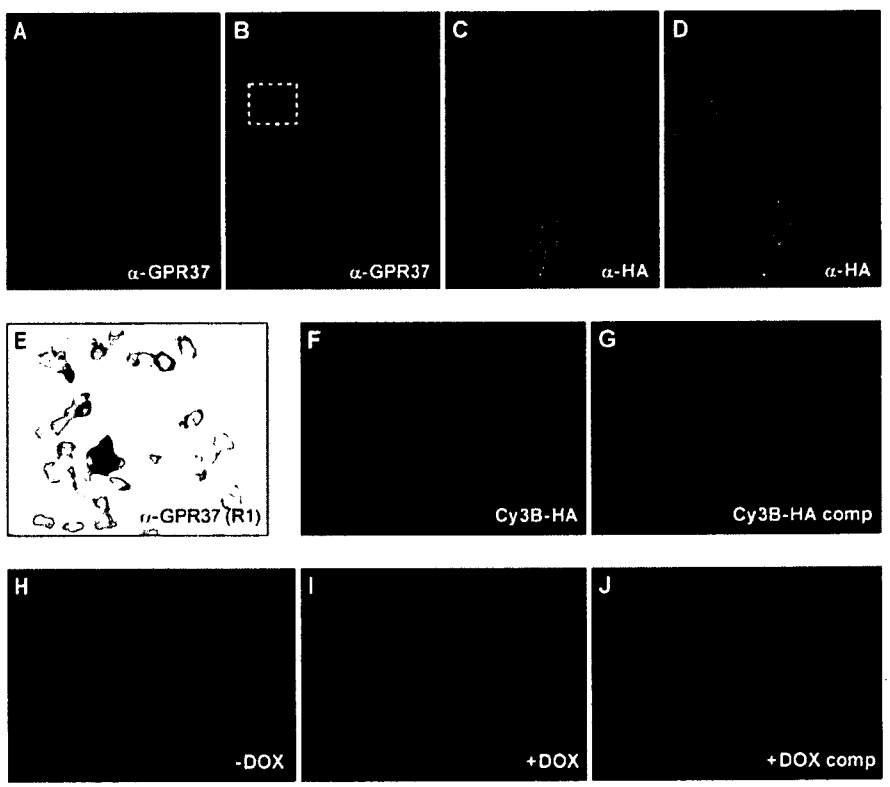

Fig. 3. HA colocalises with and binds to GPR37. (A-D) Interaction of HA and GPR37 analysed by FRET. Shown is a typical example of FRET between HA and an extracellular epitope of GPR37. COS-7 cells transiently transfected with GPR37 were treated with 2 nM HA for 20 minutes on ice to prevent internalisation, followed by incubation for 20 minute on ice with the antiserum against HA (α-HA). After fixation with 4% formaldehyde in PBS, cells were immunostained with anti-GPR37 antibody (α-GPR37). GPR37 immunoreactivity was visualised with Cy3 (A,B) and that of HA with Alexa Fluor 488 (C,D). (A) The Cy3 signal (GPR37) is shown after excitation at 568 nm. (B) A discrete area was photobleached using intense 568 nm laser. The Alexa Fluor 488 signal (HA) after excitation at 488 nm is shown before (C) and after (D) photobleaching. In this example, the Alexa Fluor 488 signal was increased by 18%. (E-G) The neuroblastoma cell line NH15-CA2 was used as a positive control to show specific Cy3B-HA binding to endogenous HA receptors. (E) NH15-CA2 cells endogenously express GPR37, as visualised with anti-GPR37(R1) antibody [α-GPR37(R1)]. (F,G) Binding is optimal at 150 nM of Cy3B-HA after incubation for 10 minutes at 37°C (Cy3B-HA) and is inhibited by pretreatment for 50 minutes at 37°C with 100 nM unlabelled, monomerised HA (Cy3B-HA comp). (H-J) HEK-T-REx–GPR37 cells bound Cy3B-HA only after GPR37 induction with doxycycline (±DOX), and binding was competed with unlabelled HA (+DOX comp).

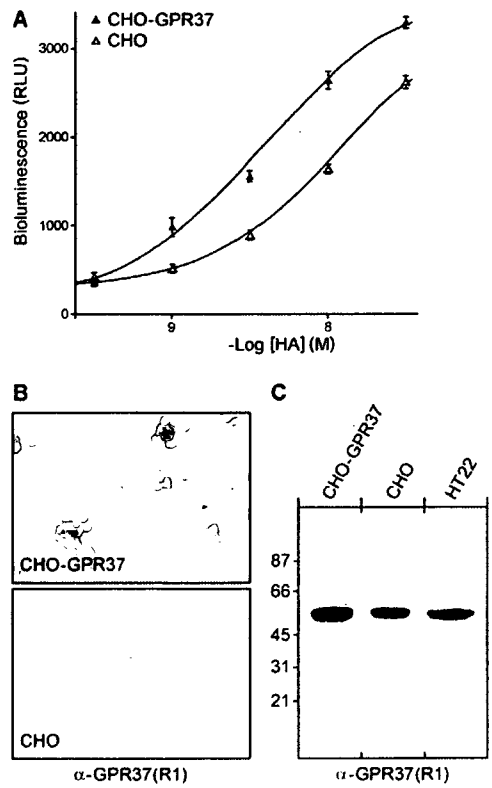

Fig. 4. HA stimulates Ca^{2+} mobilisation in CHO-K1 cells stably transfected with GPR37-FLAG, Gα16 and apoaequorin. (A) The Ca^{2+}-bioluminescence response was measured at 469 nm and is expressed in relative light units (RLU), from which the medium response was subtracted. Values are given as means ± s.d. CHO-Gα16-AEQ cells stably expressing GPR37-FLAG (CHO-GPR37) responded with an EC_{50} value of 3.3 nM; the endogenous response of CHO-Gα16-AEQ cells (CHO) resulted in an EC_{50} value of 11 nM. Data show representative results of three independent experiments. (B) CHO-GPR37 (upper panel) and CHO cells (lower panel) reacted with anti-GPR37(R1) antibody [α-GPR37(R1)], a polyclonal antiserum produced against the conserved intracellular C-tail. (C) Western blot analysis of membrane fractions confirmed an increased expression of GPR37 in transfected cells. The mouse hippocampal cell line HT22, expressing GPR37 endogenously, was used as a positive control.

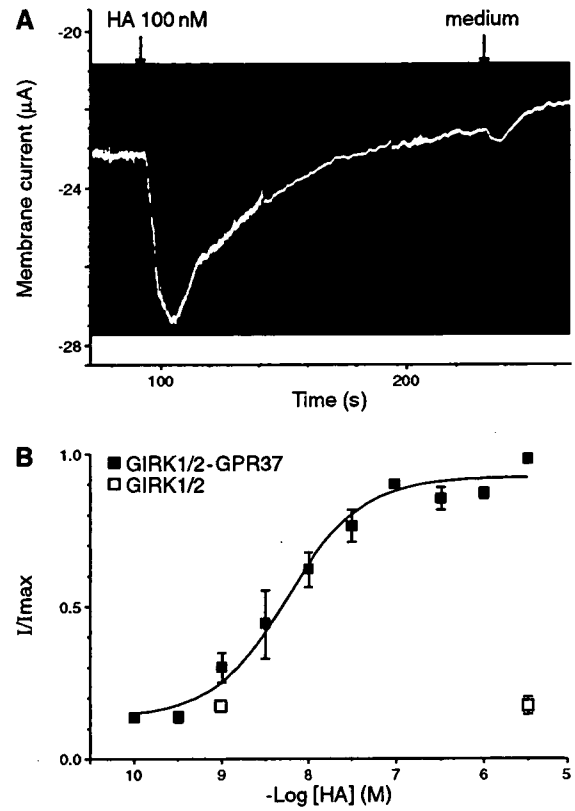

Fig. 5. HA is a high-affinity ligand for GPR37 expressed in frog oocytes. (A) Currents induced by 100 nM HA were recorded from *Xenopus* oocytes injected with cRNAs coding for GPR37 and for GIRK1/2. Stimulation with medium served as control. (B) The current increase was dependent on HA concentration. Dose-response curves for a HA-induced increase in GIRK1/2-mediated inward currents were normalised against maximal currents obtained for each oocyte. Current increases were averaged over four oocytes prepared and injected on the same day. The values represent means ± s.d. Data are representative of several independent experiments.

to an increase in membrane currents (Fig. 6B), which was blocked by La^{3+} and by SKF (Fig. 6B), both of which are known inhibitors of TRP-like Ca^{2+} channels. These Ca^{2+} channels, upon stimulation of receptors with ligands, translocate from an intracellular pool to the plasma membrane, for which activation of phosphoinositide 3-kinase (PI 3-kinase) and Ca^{2+}-dependent calmodulin (CaM) kinase is a prerequisite (Boels et al., 2001). The HA-induced increase in current was prevented by pre-incubating cells with pertussis toxin, wortmannin and KN93 (Fig. 6C), which demonstrates that an inhibitory G protein, PI 3-kinase and CaM-kinase II, respectively, are involved in the HA-GPR37 signalling cascade. A preliminary scheme of HA signalling is shown in Fig. 7.

Discussion

We present evidence that HA is a high-affinity ligand for GPR37. After heterologous expression in frog oocytes and in mammalian cells, EC_{50} values in the low nanomolar range were obtained. Electrophysiological analysis revealed that GPR37 activation by HA involved the same signalling cascade (Fig. 7) as found earlier for the endogenous HA receptor (Boels et al., 2001; Kayser et al., 1998; Ulrich et al., 1996). Interaction with HA resulted in GPR37 internalisation and stimulated entry into mitosis.

HA is bound to a carrier-like molecule both in hydra and in mammals, which improves the half-life and function of HA (Roberge et al., 1984; Schaller et al., 1996). The HA-binding protein HAB was isolated from hydra using HA-affinity chromatography, and later SorLA was discovered as an orthologue of HAB (Hampe et al., 2000). SorLA is a multi-ligand sorting receptor that, in addition to HA, binds glial-cell-derived neurotrophic factor (GDNF), PDGF and apolipoprotein E (ApoE) (Gliemann et al., 2004; Taira et al., 2001; Westergaard et al., 2004). HAB and SorLA are type I

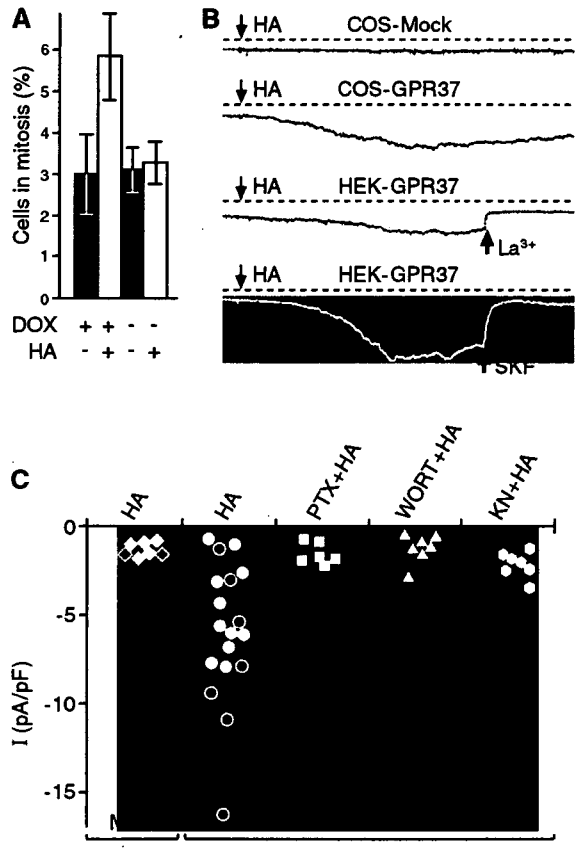

Fig. 6. GPR37 mediates HA signalling to stimulate mitosis. (A) HEK-T-REx–GPR37 cells were treated with and without doxycycline for 24 hours. Incubation with 2 nM HA for 1.7 hours led to an increase of cells in mitosis after induction of GPR37 expression. Immunostaining of cells with anti-phospho-histone H3 (1:1000) was used to determine cells in mitosis. 6×350 cells were counted, and the percentage of stained mitotic cells is given as means ± s.d. (B) Membrane currents were measured in the perforated patch configuration at a holding potential of –80 mV. Treatment with 1 nM HA induced an increase in membrane currents in COS-7 cells transiently expressing GPR37 (COS-GPR37), but not in mock-injected cells (COS-Mock). Membrane currents activated by HA in HEK-T-REx–GPR37 cells were blocked by application of 1 mM La^{3+} or 10 μM SKF. (C) Membrane-current densities were recorded from mock- and GPR37-transfected COS-7 cells. HA signal transduction was inhibited by pretreating cells for 2-3 hours with 200 ng ml^{-1} pertussis toxin (PTX), for 30-60 minutes with 100 nM wortmannin (WORT), or 30 μM KN93 (KN). Each symbol represents one cell measured in the whole-cell (filled symbols) or the perforated patch (open symbols) configuration

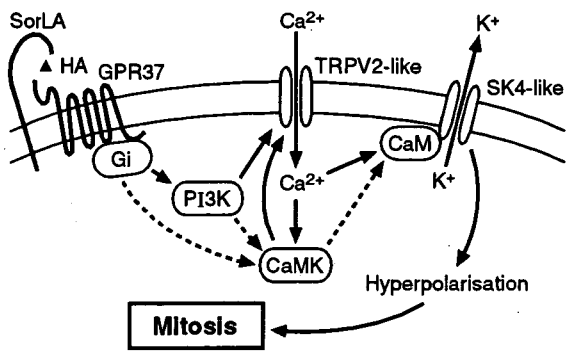

Fig. 7. Scheme of the signalling pathway from HA through GPR37 to stimulate mitosis. After binding of HA to GPR37 with or without help of the coreceptor SorLA, a pertussis-toxin-sensitive inhibitory G protein (Gi) is activated, which interacts through the phosphoinositide 3-kinase (PI3K) and the calcium-calmodulin dependent kinase II (CaMK) with a Ca^{2+} channel of the transient receptor potential family (TRPV2-like). The resulting Ca^{2+} influx activates a Ca^{2+}-dependent K^+ channel of the small and intermediate conductance family (SK4-like), leading to hyperpolarisation, which is a prerequisite for cells to enter mitosis. Dashed lines indicate hypothetical pathways.

transmembrane receptors with a large extracellular domain that can be shed by metalloprotease cleavage (Hampe et al., 2000). This represents an ideal mechanism to regulate the range of action of a morphogen like HA. GPR37 contains a relatively large extracellular domain, which is unusual for a peptide receptor. The notion that SorLA interacts with this domain of GPR37 as co-receptor to enhance HA binding (Hampe et al., 2000) is plausible and outlined in Fig. 7.

GPCRs play key physiological roles, and their dysfunction is implicated in several diseases. This might be reflected by the fact that about half of the current drugs, and certainly more in the future, are targeted to these receptors. GPR37 is of special interest for pharmacology, since it was shown to contribute to Parkinson's disease. GPR37 was characterised as a substrate for the E3 ubiquitin ligase parkin (Imai et al., 2001). Ubiquitylation marks proteins for degradation. Parkin mutations have been shown to be causative for neurodegeneration in Parkinson's disease, where dopaminergic neurons of the substantia nigra are especially affected (Imai et al., 2001; Yang et al., 2003). We found that overexpression of GPR37 resulted in complexes of molecular masses ≥250 kDa. Aggregated GPR37 did not translocate to the cell surface, as shown by cell-surface biotinylation experiments, and most probably led to preferential cell death of transfected cells. We could express GPR37 successfully in frog oocytes and in mammalian cells after stable integration into the chromosome. Since frog oocytes are cultured at room temperature, more time for proper folding may have been advantageous for GPR37 expression. Similarly, lower levels of GPR37 transcripts by stable expression may have caused less stress for the cells. The fact that insoluble GPR37 was enriched in brains of patients with juvenile Parkinson's disease (Imai et al., 2001) and its presence in Lewy bodies (Murakami et al., 2004) supports the notion that GPR37 misfolding contributes to neuronal cell death (Imai et al., 2003). This might be confirmed by the recent finding that GPR37-knockout mice showed altered dopaminergic signalling and were resistant to the neurotoxin 1-methyl-4-phenyl-1,2,3,6-tetrahydropyridine (MPTP), which preferentially kills dopaminergic neurons (Marazziti et al., 2004). As SorLA was found to be downregulated in the brains of patients with Alzheimer's disease (Scherzer et al., 2004), it is intriguing to speculate that a connection exists between SorLA, GPR37 and HA to improve neuronal cell survival.

Materials and Methods

Monomerisation of HA and synthesis of Cy3B-labelled HA

HA was from Bachem AG. Monomerisation was achieved by heating a 10 μM solution of HA in 0.1 N HCl for 5 minutes to 95°C. After neutralisation with NaOH to pH 7.0, samples were stored frozen at –20°C and used 2-3 times only (Bodenmuller et al., 1986). For labelling Cy3B, 150 nmoles of monomerised HA were lyophilised and dissolved in 100 μl dimethylformamide containing 0.2% *N*-methylmorpholine. Cy3B-mono-*N*-hydroxysuccinimide (NHS) ester (Amersham Biosciences) was dissolved in the same buffer (0.5 mg in 50 μl) and incubated with HA overnight in the dark. The Cy3B-labelled HA was purified by C18 reverse-phase HPLC, yielding approximately 30-40 nmoles of Cy3B-labelled HA.

Molecular biology

Human GPR37 cDNA was inserted into pcDNA 3.1 (+) and into pcDNA3-FLAG-His6C as described earlier (Imai et al., 2001). GPR37 and GPR37-FLAG were subcloned into the dual-function vector pXOON, a kind gift from T. Jespersen, optimised for expression both in frog oocytes and in mammalian cells (Jespersen et al., 2002). GPR37-FLAG was introduced into CHO-K1 cells stably expressing Gα16 and apoaequorin (CHO-Gα16-AEQ) (Stables et al., 1997) with the vector pIRES-P, a kind gift from S. Hobbs (Hobbs et al., 1998). Stable integration was monitored by immunostaining with antibodies against FLAG (Sigma-Aldrich). For inducible expression, GPR37 was transfected into HEK-293 cells using the Flp-In T-REx system of Invitrogen (Karlsruhe, Germany). The concatemeric construct between GIRK1 and GIRK2 (GIRK1/2) was kindly provided by A. Karschin (Wischmeyer et al., 1997). All constructs were confirmed by sequencing.

Expression of GPR37 in *Xenopus laevis* oocytes and electrophysiology

For functional expression in frog oocytes, the GPR37 cRNA was transcribed in vitro with T7 polymerase from the *XbaI*-linearised pXOON-GPR37-FLAG vector and co-injected at a ratio of 5:1 with cRNA of the concatemeric GIRK1/2 construct transcribed from the *NheI*-linearised plasmid. For recordings, oocytes were superfused with ND-96 medium (96 mM NaCl, 2 mM KCl, 1.8 mM $CaCl_2$, 1 mM $MgCl_2$, 5 mM Hepes, pH 7.5). Two-electrode voltage-clamp recordings were performed with electrodes pulled to a tip resistance of 0.5-2.0 MΩ. A Gene Clamp 500B amplifier (Axon Instruments), pClamp9 (Axon Instruments) and Origin (Microcal Software) served for data acquisition and analysis. Whole cells were clamped at –100 mV. For agonist measurements, the medium was changed to high K^+ (ND-96 with 96 mM KCl, 2 mM NaCl). After the initial inward current had reached a plateau, agonists were applied in high K^+ medium. Agonist treatment was terminated by wash-out with low K^+ to control intactness of the oocyte membrane. All recordings were performed at room temperature.

Cell culture, transfection and immunostaining

NH15-CA2, HT22 and COS-7 cells were cultured in DMEM supplemented with 10% fetal calf serum (FCS), HEK-T-REx-GPR37 cells with 10% newborn calf serum (tetracycline-free) and CHO-K1 cells in DMEM-F12 with 5% FCS. For routine culture, 100 U ml^{-1} penicillin, 100 μg ml^{-1} streptomycin and 10 mM Hepes, pH 7, were added to these media. CHO-Gα16-AEQ cells stably expressing GPR37 required the addition of 750 μg ml^{-1} geneticin, 200 μg ml^{-1} hygromycin and 5 μg ml^{-1} puromycin. HEK-T-REx-GPR37 cells were induced to express GPR37 by incubation in 1 μg ml^{-1} doxycycline. Lipofectamine 2000 (Invitrogen), Fugene 6 (Roche Diagnostics), or electroporation were used for transfection. To assay ligands, cells were transferred overnight into serum-free defined medium consisting of the respective basal media to which 5 μg ml^{-1} insulin, 30 μg ml^{-1} transferrin, 20 μM ethanolamine, 30 nM sodium selenite, 1 μM sodium pyruvate, 1% non-essential amino acids and 2 mM glutamine were added.

For immunocytochemistry, cells were fixed either with 4% formaldehyde in PBS for 30 minutes at room temperature or with ice-cold 1% acetic acid in ethanol for 5 minutes. After washing with 0.1% Triton X-100 and pre-absorption with 1% bovine serum albumin, first and second antibodies were applied. For cell-surface staining, living cells were incubated with ligand and/or antisera for 20-30 minutes on ice, washed, fixed and visualised as indicated. No Triton X-100 was added to prevent permeabilisation. For western blotting, cells were harvested by treatment with 2 mM EDTA in PBS for 10 minutes, collected by centrifugation, and ultrasonicated for 20 seconds in Tris-HCl buffer, pH 7.4, containing 2 mM EDTA and a protease-inhibitor cocktail (Roche Diagnostics). After centrifugation at 100,000 *g*, the membrane pellets were dissolved in sample buffer and separated by SDS-PAGE. The monoclonal mouse anti-GPR37 antibody, recognising an extracellular domain of recombinant human GPR37, was used at a dilution of 1:400, the polyclonal rabbit antisera against the intracellular C-terminal domain of GPR37, anti-GPR37(R1) and anti-GPR37(R2), were diluted 1:1000 and 1:2000, respectively. All GPR37-specific antibodies were produced in the laboratory of Takahashi and have been described previously (Imai et al., 2001). The antibody against FLAG (M2) was from Sigma-Aldrich and that against phospho-histone H3 from Biomol. Cy2 or Cy3 secondary antibodies were used for confocal analysis, and alkaline phosphatase- or peroxidase-conjugated secondary antibodies were used for light microscopy and western blotting. Western blots were visualised by ECL. Biotinylated proteins were detected with an avidin-peroxidase conjugate (Bio-Rad).

FRET analysis

For fluorescence resonance energy transfer (FRET) experiments, HA was reacted with the highly specific HA antiserum 102.8, which binds to HA in the picomolar range and was described earlier (Schaller et al., 1984). It was used at a dilution of 1:3000 and visualised with Alexa Fluor 488 goat anti-rabbit as donor (Invitrogen). GPR37 was detected with anti-GPR37 antibody and visualised with Cy3 anti-mouse antibody (Amersham) as acceptor. The energy transfer was detected as increase in donor fluorescence (Alexa Fluor 488) after complete photobleaching of the acceptor molecule (Cy3). Initial images were recorded after excitation at 488 and 568 nm. A discrete area of the sample was illuminated with intense 568 nm light (laser power 100%) for a few minutes to destroy completely the acceptor fluorescence. The cell was then rescanned using excitation at 488 nm. An increase within the photobleached area was used as a measure for the amount of FRET obtained. The efficiency of energy transfer (E) was expressed as E=1-(D1/D2), where D1 is the donor fluorescence before, and D2 after, photobleaching. Data were collected for 4-5 different fields from a single coverslip; 2-3 coverslips were used for each measurement; the experiment was repeated at least three times.

Biotinylation of surface proteins

COS-7 cells were transiently transfected with GPR37-FLAG using the Fugene 6 reagent (Roche Diagnostics). 48 hours after transfection, cells were washed 2× with PBS and biotinylated for 30 minutes at room temperature with 1 mM S-NHS-biotin (Perbio Science). The reaction was stopped by addition of 0.5 M Tris-HCl, pH 7.5, for 5 minutes at room temperature, and the cells were washed with PBS to remove free biotin. Cell lysates were prepared in a buffer consisting of 5 mM EDTA, 10 mM Tris-HCl, pH 7.4, and protease-inhibitor cocktail. Samples were ultrasonicated for 20 seconds and centrifuged at 100,000 *g* for 30 minutes. Pellets were solubilised in buffer containing 1% Triton X-100, 0.5% NP40, 150 mM NaCl, 7 mM EDTA, 1 mM EGTA, 10 mM Tris-HCl, pH 7.4, and protease-inhibitor cocktail for 30 minutes on ice, followed by centrifugation at 16,000 *g* for 15 minutes at 4°C. The supernatant was used for immunoprecipitation.

Immunoprecipitation with anti-FLAG M2-agarose

Since high concentrations of NP40 inhibited binding to FLAG-agarose, the supernatant from the NP40-solubilised and biotinylated COS-7 cells was diluted fivefold with TBS (150 mM NaCl, 50 mM Tris-HCl, pH 7.4) to reduce the NP40 concentration to 0.1%. Samples were incubated with 100 μl anti-FLAG M2-agarose (Sigma-Aldrich) overnight at 4°C and then centrifuged at 1500 *g* for 5 minutes at 4°C. Pellets were resuspended in 1 ml TBS and centrifuged again at 16,000 *g* for 2 minutes at 4°C. After washing with TBS, pellets were dissolved in 50 μl sample buffer and subjected to western blotting.

Electrophysiology with mammalian cells

For electrical recordings, COS-7 cells were microinjected with 50 ng μl^{-1} GPR37-pcDNA3 and 5 ng μl^{-1} EGFP-N1-pcDNA3, the latter being used to facilitate detection of successfully transfected cells. Membrane currents were recorded in the whole-cell configuration of the patch-clamp technique (Hamill et al., 1981) or the perforated-patch configuration with nystatin (Horn and Marty, 1988). An EPC9 patch-clamp amplifier was used in conjunction with the PULSE-stimulation and data-acquisition software (HEKA Elektronik). The patch electrodes were made from 1.5 mm diameter borosilicate glass capillaries with resistances of 2.5-4 MΩ. Data were low-pass filtered at 3 kHz and compensated for both fast and slow capacity transients. Series resistance was compensated by 75-90%. All experiments were performed at room temperature (22-25°C). The pipette solution contained 140 mM KCl, 2 mM $MgCl_2$, 1 mM $CaCl_2$, 2.5 mM EGTA, 10 mM HEPES and had a calculated free Ca^{2+} concentration of 66 nM. The pH was adjusted to 7.3 with KOH. The standard external solutions contained 140 mM NaCl, 2 mM $MgCl_2$, 2 mM $CaCl_2$, 5 mM KCl, 10 mM HEPES and 10 mM glucose, buffered to pH 7.3 with NaOH. Nystatin was dissolved in dimethyl sulfoxide (DMSO). Its final concentration in the standard pipette solution was 0.2 mg ml^{-1}. All chemicals for electrophysiology were purchased from Sigma-Aldrich.

Statistical analysis

The results are expressed as means of 3-6 determinations ± s.d. Curve fittings were performed with the Prism program (GraphPad). Each experiment was repeated at least three times.

We thank T. Jespersen for providing the vector pXOON, S. Hobbs for pIRES-P, A. Karschin for the concatemeric GIRK1/2 construct, J. Stables for the CHO-Gα16-AEQ cell line and S. Hempel for help with the figures.

References

Bodenmuller, H. and Schaller, H. C. (1981). Conserved amino acid sequence of a neuropeptide, the head activator, from coelenterates to humans. *Nature* **293**, 579-580.

Bodenmuller, H., Schilling, E., Zachmann, B. and Schaller, H. C. (1986). The neuropeptide head activator loses its biological activity by dimerization. *EMBO J.* **5**, 1825-1829.

Boels, K. and Schaller, H. C. (2003). Identification and characterisation of GPR100 as a novel human G-protein-coupled bradykinin receptor. *Br. J. Pharmacol.* **140**, 932-938.

Boels, K., Glassmeier, G., Herrmann, D., Riedel, I. B., Hampe, W., Kojima, I., Schwarz, J. R. and Schaller, H. C. (2001). The neuropeptide head activator induces activation and translocation of the growth-factor-regulated Ca^{2+}-permeable channel GRC. *J. Cell Sci.* **114**, 3599-3606.

Frederiksson, R., Lagerström, M. C., Lundin, L. G. and Schlöth, H. B. (2003). The G-protein-coupled receptors in the human genome form five main families. Phylogenetic analysis, paralogon groups, and fingerprints. *Mol. Pharmacol.* **63**, 1256-1272.

Gliemann, J., Hermey, G., Nykjær, A., Petersen, C. M., Jacobsen, C. and Andreasen, P. A. (2004). The mosaic receptor sorLA/LR11 binds components of the plasminogen-activating system and platelet-derived growth factor-BB similarly to LRP1 (low-density lipoprotein receptor-related protein), but mediates slow internalization of bound ligand. *Biochem. J.* **38**, 203-212.

Hamill, O. P., Marty, A., Neher, E., Sakmann, B. and Sigworth, F. J. (1981). Improved patch-clamp techniques for high-resolution current recording from cells and cell-free membrane patches. *Pflügers Arch.* **391**, 85-100.

Hampe, W., Riedel, I. B., Lintzel, J., Bader, C. O., Franke, I. and Schaller, H. C. (2000). Ectodomain shedding, translocation and synthesis of SorLA are stimulated by its ligand head activator. *J. Cell Sci.* **113**, 4475-4485.

Hobbs, S., Jitrapakdee, S. and Wallace, J. C. (1998). Development of a bicistronic vector driven by the human polypeptide chain elongation factor 1Alpha promoter for creation of stable mammalian cell lines that express very high levels of recombinant proteins. *Biochem. Biophys. Res. Commun.* **251**, 368-372.

Horn, R. and Marty, A. (1988). Muscarinic activation of ionic currents measured by a new whole-cell recording method. *J. Gen. Physiol.* **92**, 145-159.

Ignatov, A., Lintzel, J., Hermans-Borgmeyer, I., Kreienkamp, H. J., Joost, P., Thomsen, S., Methner, A. and Schaller, H. C. (2003a). Role of the G-protein-coupled receptor GPR12 as high-affinity receptor for sphingosylphosphorylcholine and its expression and function in brain development. *J. Neurosci.* **23**, 907-914.

Ignatov, A., Lintzel, J., Kreienkamp, H. J. and Schaller, H. C. (2003b). Sphingosine-1-phosphate is a high-affinity ligand for the G protein-coupled receptor GPR6 from mouse and induces intracellular Ca^{2+} release by activating the sphingosine-kinase pathway. *Biochem. Biophys. Res. Commun.* **311**, 329-336.

Imai, Y., Soda, M., Inoue, H., Hattori, N., Mizuno, Y. and Takahashi, R. (2001). An unfolded putative transmembrane polypeptide, which can lead to endoplasmic reticulum stress, is a substrate of Parkin. *Cell* **105**, 891-902.

Imai, Y., Soda, M., Murakami, T., Shoji, M. and Abe, K. (2003). A product of the human gene adjacent to *parkin* is a component of Lewy bodies and suppresses Pael receptor-induced cell death. *J. Biol. Chem.* **278**, 51901-51910.

Jespersen, T., Grunnet, M., Angelo, K., Klaerke, D. A. and Olesen, S. P. (2002). Dual-function vector for protein expression in both mammalian cells and *Xenopus laevis* oocytes. *BioTechniques* **32**, 536-540.

Kanzaki, M., Zhang, Y.-Q., Mashima, H., Li, L., Shibata, H. and Kojima, I. (1999). Translocation of a calcium-permeable cation channel induced by insulin-like growth factor-I. *Nat. Cell Biol.* **40**, 339-344.

Kayser, S. T., Ulrich, H. and Schaller, H. C. (1998). Involvement of a Gardos-type potassium channel in head activator-induced mitosis of BON cells. *Eur. J.Cell Biol.* **76**, 119-124.

Kofuji, P., Davidson, N. and Lester, H. A. (1995). Evidence that neuronal G-protein-gated inwardly rectifying K^+ channels are activated by $G\beta\gamma$ subunits and function as heteromultimers. *Proc. Natl. Acad. Sci. USA* **92**, 6542-6546.

Marazziti, D., Golini, E., Gallo, A., Lombardi, M. S., Matteoni, R. and Tocchini-Valentini, G. P. (1997). Cloning of GPR37, a gene located on chromosome 7 encoding a putative G-protein-coupled peptide receptor, from a human frontal brain EST library. *Genomics* **45**, 68-77.

Marazziti, D., Golini, E., Magrelli, A., Matteoni, R. and Tocchini-Valentini, G. P. (2001). Genomic analysis of *GPR37* and related orphan G-protein coupled receptor genes highly expressed in the mammalian brain. *Curr. Genom.* **2**, 253-260.

Marazziti, D., Golini, E., Mandillo, S., Magrelli, A., Witke, W., Matteoni, R. and Tocchini-Valentini, G. P. (2004). Altered dopamine signaling and MPTP resistance in mice lacking the Parkinson's disease-associated GPR37/parkin-associated endothelin-like receptor. *Proc. Natl. Acad. Sci. USA* **101**, 10189-10194.

Ménard, L., Ferguson, S. S. G., Zhang, J., Lin, F.-T., Lefkowitz, R. J., Caron, M. G. and Barak, L. S. (1997). Synergistic regulation of β_2-adrenergic receptor sequestration: Intracellular complement of β-adrenergic receptor kinase and β-arrestin determine kinetics of internalization. *Mol. Pharmacol.* **51**, 800-808.

Murakami, T., Shoji, M., Imai, Y., Inoue, H., Kawarabayashi, T., Matsubara, E., Harigaya, Y., Sasaki, A., Takahashi, R. and Abe, K. (2004). Pael-R is accumulated in Lewy bodies of Parkinson's disease. *Ann. Neurol.* **55**, 439-442.

Niemann, S. and Schaller, H. C. (1996). Head activator and the neuroectodermal differentiation of P19 mouse embryonal carcinoma cells. *Neurosci. Lett.* **207**, 49-52.

Roberge, M., Escher, E., Schaller, H. C. and Bodenmuller, H. (1984). The hydra head activator in human blood circulation. Degradation of the synthetic peptide by plasma angiotensin-converting enzyme. *FEBS Lett.* **173**, 307-313.

Schaller, H. C., Bodenmuller, H., Zachmann, B. and Schilling, E. (1984). Enzyme-linked immunosorbent assay for the neuropeptide 'head activator'. *Eur. J. Biochem.* **138**, 365-371.

Schaller, H. C., Hermans-Borgmeyer, I. and Hoffmeister, S. A. H. (1996). Neuronal control of development in hydra. *Int. J. Dev. Biol.* **40**, 339-344.

Scherzer, C. R., Offe, K., Gearing, M., Ress, H. D., Fang, G., Heilman, C. J., Schaller, H. C., Bojo, H., Levey, A. I. and Lah, J. J. (2004). Loss of apolipoprotein E receptor LR11 in Alzheimer disease. *Arch. Neurol.* **61**, 1200-1205.

Stables, J., Green, A., Marshall, F., Fraser, N., Knight, E., Sautel, M., Milligan, G., Lee, M. and Rees, S. (1997). A bioluminescent assay for agonist activity at potentially any G-protein-coupled receptor. *Anal. Biochem.* **252**, 115-126.

Taira, K., Bujo, H., Hirayama, S., Yamazaki, H., Kanaki, T., Takahashi, K., Ishii, I., Miida, T., Schneider, W. J. and Saito, Y. (2001). LR11, a mosaic LDL receptor family member, mediates the uptake of ApoE-rich lipoproteins in vitro. *Arterioscler. Thromb. Vasc. Biol.* **21**, 1501-1506.

Ulrich, H., Tárnok, A. and Schaller, H. C. (1996). Head-activator induced mitosis of NH15-CA2 cells requires calcium influx and hyperpolarization. *J. Physiol. (Paris)* **90**, 85-94.

Westergaard, U. B., Sørensen, E. S., Hermey, G., Nielsen, M. S., Nykjær, A., Kirkegaard, K., Jacobsen, C., Gliemann, J., Madsen, P. and Petersen, C. M. (2004). Functional organization of the sortilin Vps10p domain. *J. Biol. Chem.* **279**, 50221-50229.

Wischmeyer, E., Doring, F., Wischmeyer, E., Spauschus, A., Thomzig, A., Veh, R. and Karschin, A. (1997). Subunit interactions in the assembly of neuronal Kir3.0 inwardly rectifying k+ channels. *Mol. Cell Neurosci.* **9**, 194-206.

Yang, Y., Nishimura, I., Imai, Y., Takahashi, R. and Lu, B. (2003). Parkin suppresses dopaminergic neuron-selective neurotoxicity induced by Pael-R in Drosophila. *Neuron* **37**, 911-924.

Zeng, Z., Su, K., Kyaw, H. and Li, Y. (1997). A novel endothelin receptor type-B-like gene enriched in the brain. *Biochem. Biophys. Res. Commun.* **233**, 559-567.

特集

呼吸器疾患におけるアポトーシスの最新知見

アポトーシス研究の現状と今後の展望

高橋　良輔

呼 吸 と 循 環

第54巻　第1号 別刷

2006年1月15日　発行

医学書院

特集　呼吸器疾患におけるアポトーシスの最新知見

アポトーシス研究の現状と今後の展望*

高橋良輔[1]

はじめに

アポトーシスは英国の病理学者Wylie，Kerrらによって形態学的に細胞が縮み，クロマチンが濃縮する特異な形態をとる細胞死として記載，命名された．機能的にはアポトーシスは細胞の自爆に例えられるように，シグナル伝達により積極的に引き起こされる細胞死である．多細胞生物では発生過程において，多くの細胞がアポトーシスを起こして正しい形態形成が行われることが知られており，プログラム細胞死と同義で使われることもある．一方，アポトーシスは発生過程だけでなく，成体となってからもDNA損傷を起こした細胞，不要になった炎症細胞などの除去に使われており，その阻害は癌や自己免疫疾患につながると考えられる．また，逆にアポトーシスが死ぬべきでない正常な細胞に起こると，AIDSや神経変性疾患の発症に結びつくと考えられる．

このような観点から，アポトーシスの分子レベルでの理解は様々なヒトの疾患の発症メカニズムの解明と治療法開発に非常に重要である[1]．これまでの研究により，アポトーシスはカスパーゼというシステインプロテアーゼの活性化によって起こることが明らかになってきた．

本稿では，これまでにその概略が明らかにされたアポトーシスのシグナル伝達経路の基本骨格をカスパーゼの役割を中心に述べ，ついでカスパーゼ非依存的細胞死について紹介し，さらにアポトーシスと呼吸器疾患との関連についても言及する．

アポトーシスのシグナル伝達経路(1)：内因性経路(intrinsic pathway)

この10年のアポトーシス研究で明らかになった最も重要なことの一つは，ミトコンドリアがアポトーシスのセンサーとして重要な役割を果たしている事実である[2]．細胞に様々なアポトーシス誘発刺激(栄養因子除去，酸化的ストレス，DNA障害)が加わると，ミトコンドリアの外膜の透過性上昇(mitochondrial outer membrane permeabilization：MOMP)が起こり，膜間スペースに存在する蛋白質の一部が細胞質に漏出することによって細胞死の引き金が引かれる．MOMPの分子基盤となっているのはBcl-2ファミリーに属するBaxとBakという多ドメイン蛋白質である．BAXとBAKはBH3-only proteinと呼ばれるアポトーシス誘発性Bcl-2ファミリー分子の働きによって凝集(オリゴマー化)し，その結果MOMPが生じる．MOMPが一旦起こると，ミトコンドリアの膜間スペースからシトクロムcが細胞質に放出され，アポトーシスプロテアーゼ活性化因子(APAF-1)のオリゴマー化を惹起して，アポプトソーム(apoptosome)と呼ばれる蛋白質複合体が形成される．アポプトソーム複合体はプ

* Apoptosis Research：The current status and future prospects

1 京都大学医学部神経内科(〒606-8507 京都市左京区聖護院川原町54)　Ryosuke Takahashi：Department of Neurology, Kyoto University Graduate School of Medicine

0452-3458/06/¥500/論文/JCLS

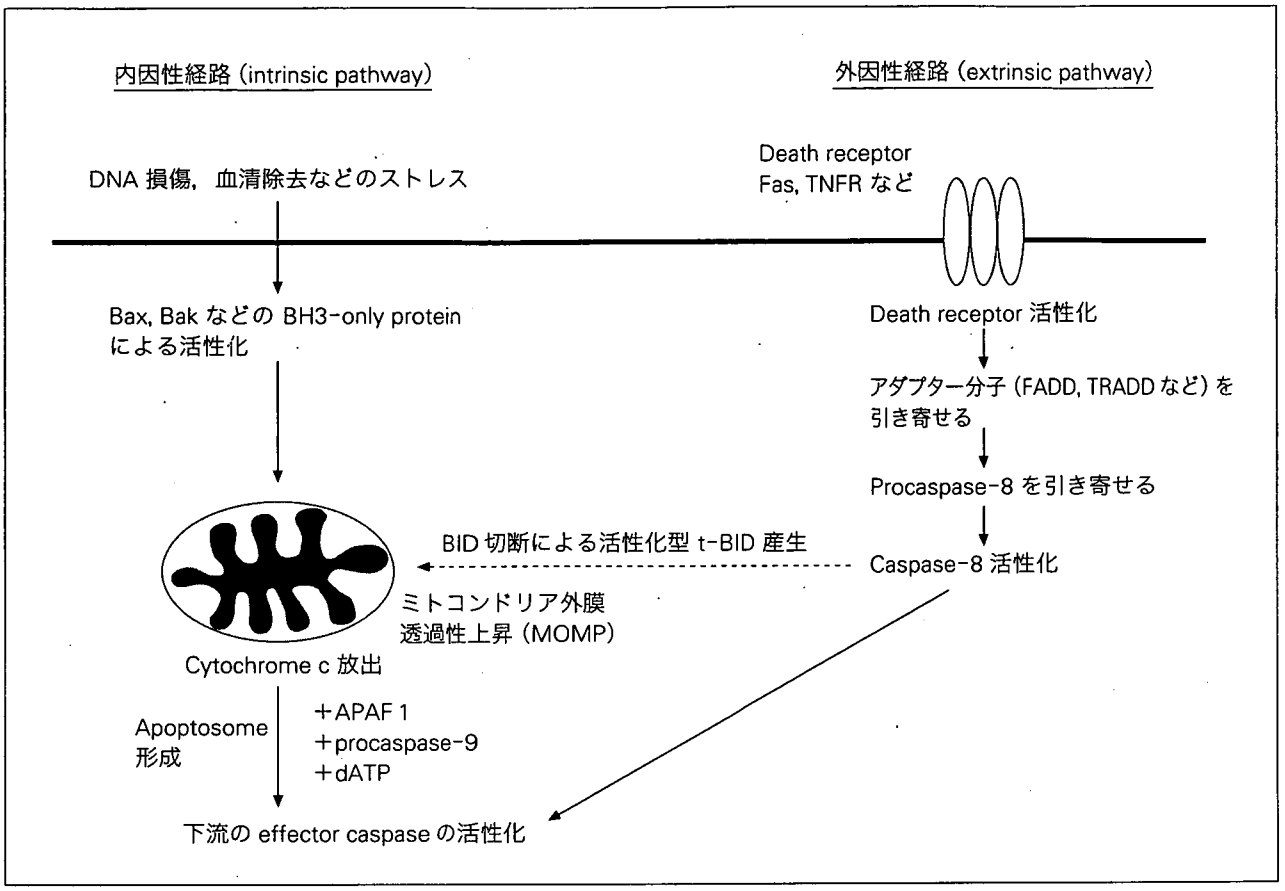

図1 アポトーシスの内因性経路と外因性経路

ロカスパーゼ9を引き寄せて活性化型のカスパーゼ-9に変換し，カスパーゼ-9は下流の実行型カスパーゼ(executioner caspase)であるカスパーゼ-3, -7などを限定分解することによって活性化し，アポトーシスが誘導される．ミトコンドリアを介するこのような経路は内因性経路(intrinsic pathway)と呼ばれており，様々な種類のアポトーシスの基本シグナルとなっている(図1)[3]．

アポトーシスのシグナル伝達経路(2)：外因性経路(extrinsic pathway)

一方，細胞膜に局在する受容体のリガンドによる刺激でアポトーシスが誘発されることも明らかになっており，これを外因性経路(extrinsic pathway)と呼ぶ(図1)．例えば，腫瘍壊死因子(TNF)がその受容体であるI型TNF受容体(TNFR 1)に結合すると，TNF-associated death domain(TRADD)やFAS-associated death domain(FADD)が引き寄せられ，プロカスパーゼ-8の結合と活性化をもたらす．この場合の活性化のメカニズムは近接誘導モデル(induced proximity model)で説明されている[4]．すなわち，不活性の前駆体であるプロカスパーゼ-8数分子がTRADDまたはFADDのようなアダプター分子の仲介によって引き寄せられ，近接化してオリゴマー形成をすることによって活性化が起こる．このようにして活性化されたカスパーゼ-8が内因性経路のカスパーゼ-9と同様の役割を果たし，実行型カスパーゼを活性化してアポトーシスを引き起こす．しかし，ある種の細胞では外因性経路に反応するだけでなく，カスパーゼ-8を介する別経路によるシグナルの増幅が必要な場合がある．これは細胞質に存在するBH 3-interacting domain death agonist(BID)というBH 3-only proteinがカスパーゼ-8によって限定分解されてt-BIDという活性型を生み出す経路である．t-BIDはBaxやBakの構造変化を引き起こして，MOMPを誘導する．このt-BIDが働く細胞では

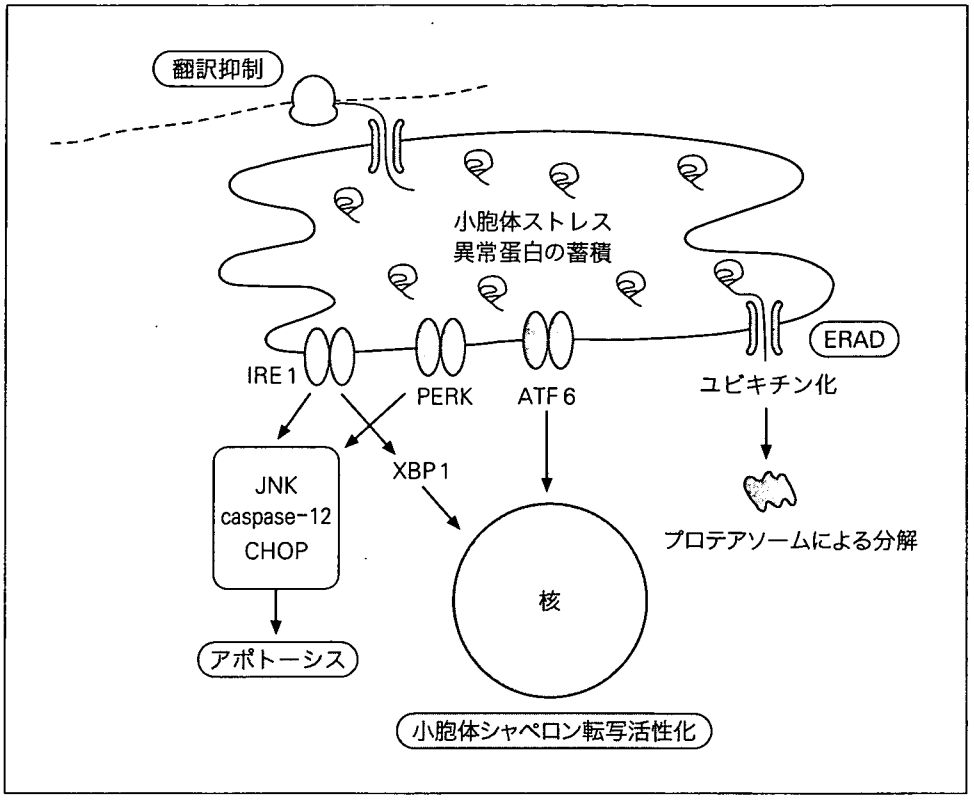

図2　小胞体ストレス応答とアポトーシスの経路

外因性経路に加えて内因性経路が利用されることになる．

アポトーシスのシグナル伝達経路(3)：小胞体経路(ER pathway)

小胞体は膜蛋白質や分泌性蛋白質の品質管理を行う細胞内小器官であり，新生した分泌系蛋白質が翻訳と共役して常に小胞体内腔に送り込まれ，小胞体シャペロンがそのような分子の折り畳み(folding)を助けている．小胞体内腔に折り畳みが完了していない(unfolded protein)または折り畳みに失敗した蛋白質(misfolded protein)が小胞体に過剰に蓄積した状態を小胞体ストレスと呼ぶ[5,6]．小胞体ストレスはストレス応答として，小胞体センサー分子IRE 1，ATF 6，PERKなどを介して，小胞体シャペロンの転写活性化，翻訳の全般的抑制などを引き起こし，ストレスを回避しようとするが，これらの手段で間に合わない場合にはアポトーシスを起こす(図2)[6]．

アポトーシスを起こす経路には諸説あるが，次の3種類の経路が有力といわれている．第1はセンサー分子IRE 1がアダプター分子TRAF 2と結合し，TRAF 2がASK 1を活性化して向細胞死的に働く蛋白質キナーゼJNKを活性化する経路である[7]．第2はATF 6経路とPERK経路の両方で転写が誘導される転写因子CHOPによる経路である[8]．CHOPの下流のシグナルはまだよくわかっていない．第3はカスパーゼ-12を介する経路である[9]．カスパーゼ-12は小胞体膜の細胞質側に存在し，小胞体ストレスの際は切断され，活性化されて小胞体から遊離し，カスパーゼ-9を活性化するらしい．カスパーゼ-12のノックアウト細胞では小胞体ストレスによる細胞死は抑制される．ヒトではカスパーゼ-12に相当するカスパーゼは配列上活性を失っているが，ヒトではカスパーゼ-4が小胞体ストレス誘起性細胞死の担い手とする報告がある[10]．

アポトーシス阻害因子とその制御

上記のようなアポトーシスはアポトーシス阻害因子(inhibitor of apoptosis proteins：IAP)と呼ばれる内因性のカスパーゼ阻害因子によって制御されることが知られている[11]．IAPはBIR(Baculovirus IAP repeat)ドメインと呼ばれる金属結

合モチーフを持つことが構造上の特徴で，8種類知られるヒトのIAPのうち，最も細胞死抑制効果が強いとされるXIAPはカスパーゼ-3,-7,-9を阻害する．ショウジョウバエのIAPは発生過程の細胞死を制御するうえで中心的な役割を果たしているが，マウスのIAPはノックアウトしても著しい表現型はなく，これが生理的役割が大きくないことを示しているのか，類似分子により補償されているためなのか，明らかではない．ただ，ヒトのミトコンドリア膜間スペースにはsecond mitochondria-derived activator of caspase(Smac)とhigh-temperature-requirement potein A2(HtrA 2)/Omiと呼ばれる2種類のIAP阻害因子が存在し，アポトーシスが起こる際にはともにMOMPによって細胞質に放出されてIAPの機能を抑制することが知られていることから，哺乳類においてもIAPはアポトーシスを常に抑制する構成的因子として一定の役割を果たしているものと考えるのが妥当である[12,13]．

カスパーゼ非依存性細胞死

アポトーシスは以上に述べてきたようにカスパーゼ依存的な細胞死を起こすが，細胞はカスパーゼの活性を抑制した状態でアポトーシス刺激を受けても死んでしまうことがある．これをカスパーゼ非依存性細胞死(caspase-independent cell death：CICD)と呼んでいる[3]．線虫のプログラム細胞死はカスパーゼに依存的であり，CICDが存在するという積極的な証拠はない．しかし脊椎動物ではカスパーゼ阻害剤の存在下やApaf-1，カスパーゼ-9，カスパーゼ-3などのミトコンドリアの下流のアポトーシスシグナル分子を欠損した細胞で，ミトコンドリアクリステの膨化や細胞質の空胞形成などを特徴とする，形態的にアポトーシスとは大きく異なる細胞死が観察される．外因性経路においても，FADDやreceptor-interacting protein(RIP)依存性にカスパーゼ活性を阻害した条件下でCICDが観察される．このシグナル経路の詳細は不明であるが，アポトーシス時にミトコンドリアから細胞質に放出されるapotposis-inducing factor(AIF)，endonuclease G，HtrA 2/Omiが関与しているとの考えもある．また，本来は生存維持の方向に働くとされるautophagyが細胞死を誘導する可能性も提示され，注目されている[14]．

呼吸器疾患とアポトーシス

呼吸器科疾患では，最近，acute respiratory distress syndrome(ARDS)，慢性閉塞性肺疾患(COPD)に伴う肺気腫，喘息，肺線維症におけるアポトーシスの関与が注目されている[15]．これらのトピックスに関しては本特集号でそれぞれの領域の専門家が論文を寄せられているので，以下にごく簡単に紹介する．ARDSでは多核白血球のアポトーシスの遅延と内皮・上皮細胞のアポトーシス増加が病因に関与していることが示唆されている[16,17]．前者には生存促進作用を持つgranulocyte colony-stimulating factor(GCSF)やgranulocye/macrophage colony-stimulating factor(GMCSF)の関与が，後者には外因性経路(Fas/Fas ligand system)，内因性経路(ストレス)，nitric oxideなどの関与が疑われている．COPDに伴う肺気腫に関しては，プロテアーゼおよびその阻害因子の不均衡，酸化的ストレス，喫煙，マクロファージ，白血球，CD8陽性T細胞による慢性炎症などが病因として挙げられている一方，肺気腫における肺胞壁の破壊には肺上皮および内皮細胞のアポトーシスが伴うことが組織学的に示されている[17]．COPDにおけるアポトーシスの誘因として直接的，間接的に喫煙と酸化的ストレスが働いているものと思われる．喘息の原因は不明だが，気道のリモデリングと気道・肺の好酸球，CD4陽性T細胞，マスト細胞の増加を伴う慢性炎症が原因に関わっていると思われる[18]．*ex vivo*の研究では，喘息患者における末梢のCD4陽性T細胞や好酸球のアポトーシスの減少が観察され，炎症を惹起しているのかもしれない．副腎皮質ステロイドの効果は，一部は炎症に関与する細胞のアポトーシスを誘導するところにあるものと思われるが，*in vivo*の研究では，この効果はβ2アドレナリン受容体アゴニストによって拮抗されるとの注目すべき報告がなされている[19]．肺線維症における線維化は，肺胞上皮細胞のアポトーシスに二次的に生じる可能性が指摘

されている[20]．肺胞上皮細胞のアポトーシスの増加は，患者でも，げっ歯類におけるbleomycin誘発性肺線維症でもみられ，後者に関してはアポトーシスも線維化もカスパーゼ阻害剤によって抑制される．肺胞上皮細胞のアポトーシスにはFasによる外因性経路，アンジオテンシン，活性化T細胞が産生するperforin，interleukin-13刺激，transforming growth factor β1の活性化などの関与が示唆されている[21]．

おわりに

アポトーシスと関連する細胞死の基本的なシグナル経路が解明され，様々な呼吸器疾患との関わりも最近明らかになってきた．一般的に言って，肺構造の破壊は肺上皮および内皮細胞の細胞死増加と炎症細胞のアポトーシス阻害によって引き起こされるようである．したがって，アポトーシスの阻害は強力な治療法になりうるが，タイミングよく，細胞特異的に効果が得られるように行わないと重大な副作用を来す恐れがある．今後は疾患におけるアポトーシスの役割の詳細をさらに明らかにし，分子メカニズムの正確な理解に基づいた治療法を開発する必要がある．

〔謝辞：図の作成に協力してくれた田代善崇君(京都大学大学院医科学修士課程)に感謝します．〕

文　献

1) Rudin CM, Thompson CB: Apoptosis and disease: regulation and clinical relevance of programmed cell death. Annu Rev Med 48: 267-281, 1997
2) Green DR, Reed JC: Mitochondria and apoptosis. Science 281: 1309-1312, 1998
3) Chipuk JE, Green DR: Do inducers of apoptosis trigger caspase-independent cell death? Nat Rev Mol Cell Biol 6: 268-275, 2005
4) Salvesen GS, Dixit VM: Caspase activation: the induced-proximity model. Proc Natl Acad Sci USA 96: 10964-10967, 1999
5) Mori K: Frame switch splicing and regulated intramembrane proteolysis: key words to understand the unfolded protein response. Traffic 4: 519-528, 2003
6) Yoshida H, Okada T, Haze K, et al: Endoplasmic reticulum stress-induced formation of transcription factor complex ERSF including NF-Y(CBF) and activating transcription factors 6alpha and 6beta that activates the mammalian unfolded protein response. Mol Cell Biol 21: 1239-1248, 2001
7) Nishitoh H, Matsuzawa A, Tobiume K, et al: ASK1 is essential for endoplasmic reticulum stress-induced neuronal cell death triggered by expanded polyglutamine repeats. Genes Dev 16: 1345-1355, 2002
8) Oyadomari S, Mori M: Roles of CHOP/GADD153 in endoplasmic reticulum stress. Cell Death Differ 11: 381-389, 2002
9) Momoi T: Caspases involved in ER stress-mediated cell death. J Chem Neuroanat 28: 101-105, 2004
10) Hitomi J, Katayama T, Eguchi Y, et al: Involvement of caspase-4 in endoplasmic reticulum stress-induced apoptosis and Abeta-induced cell death. J Cell Biol 165: 347-356, 2004
11) Salvesen GS, Duckett CS: IAP proteins: blocking the road to death's door. Nat Rev Mol Cell Biol 3: 401-410, 2002
12) Du C, Fang M, Li Y, et al: Smac, a mitochondrial protein that promotes cytochrome c-dependent caspase activation by eliminating IAP inhibition. Cell 102: 33-42, 2000
13) Suzuki Y, Imai Y, Nakayama H, et al: A serine protease, HtrA2, is released from the mitochondria and interacts with XIAP, inducing cell death. Mol Cell 8: 613-621, 2001
14) Tsujimoto Y, Shimizu S: Another way to die: autophagic programmed cell death. Cell Death Differ 12(Suppl 2): 1528-1534, 2005
15) de Souza PM, Lindsay MA: Apoptosis as a therapeutic target for the treatment of lung disease. Curr Opin Pharmacol 5: 232-237, 2005
16) Matute-Bello G, Martin TR: Science review: apoptosis in acute lung injury. Crit Care 7: 355-358, 2003
17) Yokohori N, Aoshiba K, Nagai A: Increased levels of cell death and proliferation in alveolar wall cells in patients with pulmonary emphysema. Chest 125: 626-632, 2004
18) Jayaraman S, Castro M, O'Sullivan M, et al: Resistance to Fas-mediated T cell apoptosis in asthma. J Immunol 162: 1717-1722, 1999
19) Tse R, Marroquin BA, Dorscheid DR, White SR: Beta-adrenergic agonists inhibit corticosteroid-induced apoptosis of airway epithelial cells. Am J Physiol Lung Cell Mol Physiol 285: L393-404, 2003
20) Uhal BD, Joshi I, Hughes WF, et al: Alveolar epithelial cell death adjacent to underlying myofibroblasts in advanced fibrotic human lung. Am J Physiol 275: L1192-1199, 1998
21) Lee CG, Cho SJ, Kang MJ, et al: Early growth response gene 1-mediated apoptosis is essential for transforming growth factor beta1-induced pulmonary fibrosis. J Exp Med 200: 377-389, 2004

AMPA 受容体と変異 SOD 1 タンパク質異常

舘野美成子　高橋良輔

CLINICAL NEUROSCIENCE 別冊

Vol. 24 No. 2　2006 年 2 月 1 日発行

中 外 医 学 社

グルタミン酸受容体と神経疾患

AMPA受容体と変異SOD1タンパク質異常

舘野 美成子　高橋 良輔

▣ はじめに

筋萎縮性側索硬化症amyotrophic lateral sclerosis (ALS)は，上位および下位運動ニューロンが選択的かつ系統的に障害される代表的な進行性神経変性疾患である[1]．有病率は人口10万人当たり2～7人で，患者の多くは孤発性だが約10%は家族性を示す．1993年に家族性ALSの最初の原因遺伝子としてスーパーオキシドジスムターゼ1 superoxide dismutase 1(SOD1)が同定されて以来，変異SOD1はALS発症分子機構を解く鍵として精力的に研究されてきた[1,2]．本稿では，家族性ALSのモデルマウスである変異SOD1トランスジェニックマウスにおいて，下位運動ニューロンで特異的に発現しているカルシウム透過型AMPA受容体が，変異SOD1タンパクの構造変換を促進しALS発症を促す因子であることを紹介する．

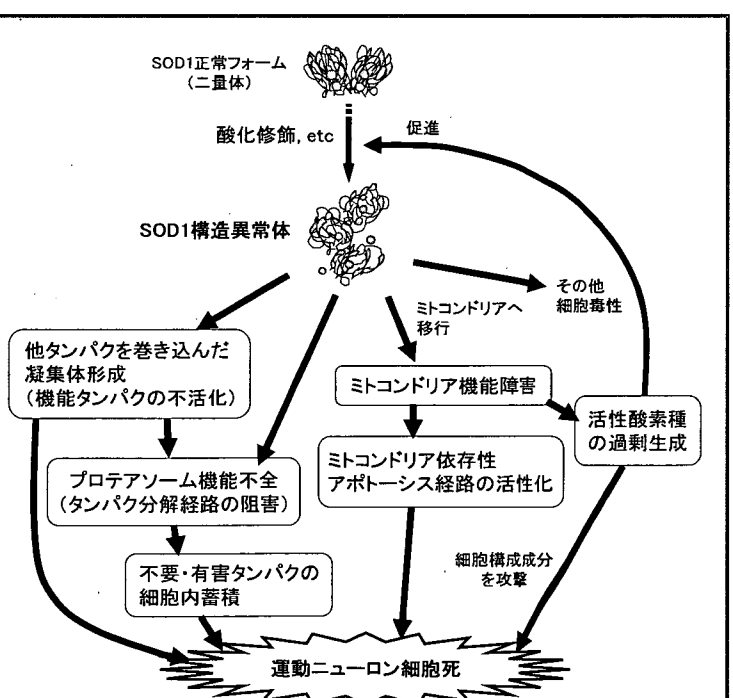

図1　変異SOD1タンパクの細胞毒性：異常タンパク仮説
変異SOD1タンパクは立体構造が不安定で，酸化修飾を受けると凝集化が促進される[3,4]．このような構造異常体は，主にミトコンドリアやプロテアソームの機能障害を引き起こすことで運動ニューロン変性を導くと考えられている[2]．

変異SOD1タンパクの細胞毒性：異常タンパク仮説

SOD1は真核細胞の細胞質で主力となる活性酸素除去酵素で，酸素呼吸の副産物として生成されるスーパーオキシド($\cdot O_2^-$)の過酸化水素への変換を触媒する[1]．このSOD1遺伝子の変異が家族性ALSの原因として発表された当時は，誰もがSOD1活性の低下がALSの発症要因と考えたことであろう．しかしその予想は見事に打ち砕かれた．これまでの研究より，ALSを引き起こすSOD1変異は機能獲得型(gain-of-function)であること，即ち，変異によってSOD1タンパクが新たに獲得した(未知の)毒性によることが示されている[1,2]．

図1に変異SOD1タンパクの毒性として最も支持されている仮説：異常タンパク仮説を紹介する[2,3]．これは変異SOD1タンパクの立体構造が変化して凝集化したもの，または凝集途上の中間体(構造異常体)が細胞毒性を有し，運動ニューロン変性が引き起こされる，という考え方である．SOD1はわずか153個のアミノ酸からなる小さなタンパクだが，ALS患者から同定された変異は100種類以上に及び，変異箇所はタンパクのほぼ全域に散在している．変異SOD1タンパクの多くは立体構造が不安定化で凝集しやすく，酸化修飾を受けると巨大な凝集塊を形成しうることが示されている[3,4]．SOD1構造異常体が有する細胞毒性の実態はまだ明らかにされていないが，SOD1変異をもつ家族性ALS患者やトランスジェニックマウスの残存脊髄運動ニューロン内には抗SOD1抗体陽性の凝集体が観察されており[5,6]，このことからも異常タンパク仮説が強く支持

たての みなこ　国立精神・神経センター神経研究所/疾病研究第5部室長
たかはし りょうすけ　京都大学教授/大学院医学研究科臨床神経学

0289-0585/06/¥500/論文/JCLS

カルシウム透過型 AMPA 受容体の減少による ALS 発症遅延と延命効果

chat-GluR2-Tg ライン	Transgene コピー数	GluR 2 発現量[a]		*chat-GluR2*-Tg *x* *hSOD1*^{G93A}-Tg で得られた littermates 間での発症時期[b]・生存期間の比較(日齢, Mean±SEM)			
				hSOD1^{G93A}/+	*chat-GluR2*/+ ; *hSOD1*^{G93A}/+	GluR 2 増加による遅延効果	*p* value[c]
Tg 7	10	0.96	発症時期	219.7±3.0	262.2±2.9	+42.5(=19.3%)	0.0001
			生存期間	262.5±4.5	300.1±3.9	+37.6(=14.3%)	0.0001
Tg 10	16	4.78	発症時期	219.8±2.6	238.5±2.7	+18.7(=8.6%)	0.0001
			生存期間	264.5±2.2	279.7±3.1	+15.2(=5.8%)	0.0005
Tg 3	2	1.58	発症時期	225.6±1.0	230.4±1.0	not significant	>0.05
			生存期間	267.1±5.1	273.3±5.2		

[a] 脊髄運動ニューロンにおける *GluR2* mRNA 総量を定量化し, non-transgenic littermates における発現量(=1.0)に対する相対値として表記.

[b] Rotarod test におけるスコア(運動能力)が急低下する時期として判定.

[c] 各遺伝子型 littermates 10〜15 匹における値を ANOVA+*post hoc* Fisher's PLSD 法で検定.

脊髄においてほぼ運動ニューロン特異的に GluR 2 遺伝子を過剰発現するトランスジェニックマウス; *chat-GluR2*-Tg と家族性 ALS モデルマウス; *hSOD1*^{G93A}-Tg とのダブルトランスジェニックマウスでは, GluR 2 発現量に応じて発症時期と生存期間の延長が認められた[9].

されている.

カルシウム透過型 AMPA 受容体による ALS 発症促進効果

しかし, なぜ病変部位でのみ変異 SOD 1 タンパクの凝集化が認められるのだろうか. SOD 1 変異をもつ ALS 患者やトランスジェニックマウスでは, 変異タンパクはもちろん全身の細胞で発現している. にも関わらず, 変異 SOD 1 が病変部位特異的に構造変換・蓄積するならば, 細胞種特異的な促進要因があるはずである. この問題に対して我々は, 孤発性 ALS に対して以前から提唱されていたグルタミン酸仮説に注目した[7,8]. シナプス間隙に放出されたグルタミン酸はシナプス後細胞膜上のグルタミン酸受容体に結合・活性化することで興奮性刺激を伝えるが, グルタミン酸受容体の過度の刺激は神経細胞死を引き起こす(神経興奮毒性). グルタミン酸に対する脆弱性は神経細胞の種類によって異なるが, ALS で障害される脊髄運動ニューロンはグルタミン酸に対して極めて脆弱であること, 孤発性 ALS 患者の脳脊髄液中ではグルタミン酸濃度が上昇していることなどから, ALS における運動ニューロン変性にグルタミン酸毒性が関与している可能性が指摘されていた. さらに薬理学的解析から, 脊髄運動ニューロンの高いグルタミン酸脆弱性はカルシウム透過型の AMPA 受容体を介していることが示唆された. AMPA 受容体は通常カルシウム非透過型だが, 脊髄運動ニューロンを含む, ごく限られたニューロンではカルシウム透過型も発現しているのである.

そこで我々は, このカルシウム透過型 AMPA 受容体と ALS における運動ニューロン変性との関係を追及することにした. AMPA 受容体は 4 種類のサブユニット GluR 1-4 がランダムに会合した 4 量体であり, カルシウム透過性は通常 GluR 2 サブユニットの有無で決定される. 即ち GluR 2 を含む受容体は非透過型, 含まずに会合すると透過型となる. 我々は脊髄運動ニューロンの GluR 2 発現量を特異的に上げることにより AMPA 受容体のカルシウム透過性が低下したトランスジェニックマウス(*chat-GluR2*-Tg)を作成した[9]. そして代表的な ALS モデルマウスである *hSOD1*^{G93A}-Tg(93 番目のグリシンをアラニンに置換したヒト変異 SOD 1 遺伝子を導入)と交配し, ALS 発症時期・生存期間について littermates 間で比較した(表). GluR 2 発現量が最も増大したライン(Tg 7: 野生型マウスの約 5 倍)では, 脊髄運動ニューロンにおける AMPA 受容体の大半がカルシウム非透過型を示し, 発症時期が 42.5 日(=19.3%), 生存期間が 37.8 日(=14.3%)も遅延することがわかった. GluR 2 発現量の低いラインでは発症遅延・延命効果も低く, AMPA 受容体のカルシウム透過性と発症までの期間には相関関係が認められた. 一方, AMPA 受容体をカルシウム透過性にする変異(RNA 編集部位のアミノ酸をアスパラギンに置換)をもつ GluR 2 遺伝子を導入したトランスジェニックマウスでは, 中年以降に ALS 様の運動能力低下を示すこと, さらにこの Tg マウスや GluR 2 ノックアウトマウスを *hSOD1*^{G93A}-Tg と交配すると発症が早まり, 生存期間が短縮されることが報告された[10,11]. これらの結果より, カルシウム透過型 AMPA 受容

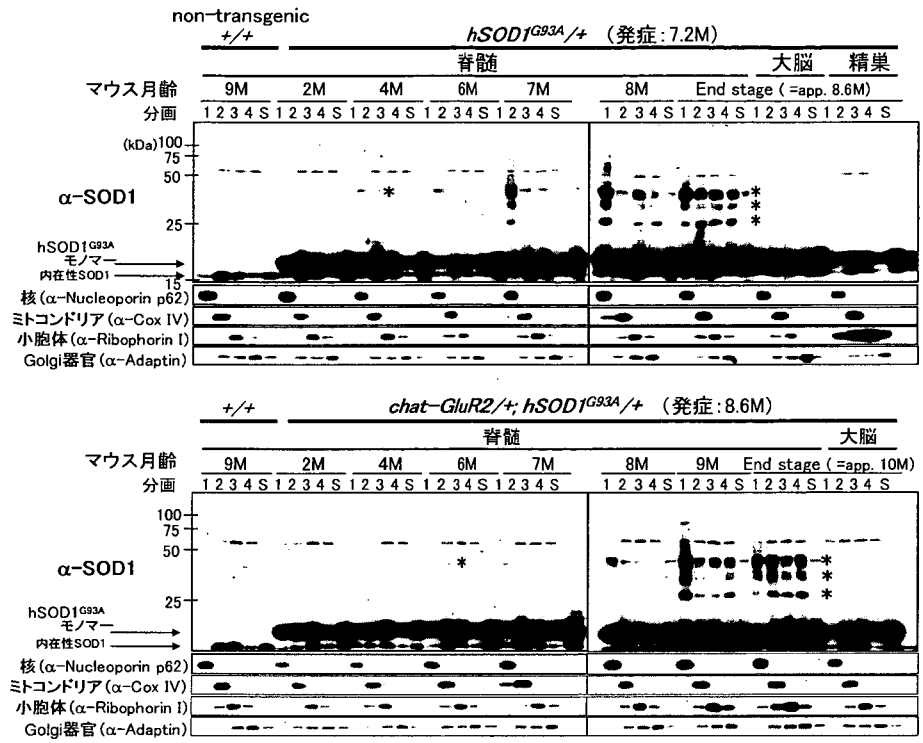

図 2　カルシウム透過型 AMPA 受容体の減少による SOD 1 構造異常体形成遅延

マウス脊髄を等張液中で破砕後遠心分離し，1：核，2：ミトコンドリア，3：ミクロソーム(小胞体膜断片等)，4：Golgi 器官，S：細胞質可溶性タンパク，を主に含む 5 つの分画に分け，ウェスタンブロット法により各分画における SOD 1 タンパクのサイズ変化を調べた．*hSOD1*^{G93A}-Tg では発症に大幅に先行して 4ヵ月齢から分画 1・2 に SOD 1 構造異常体(＊)の蓄積が認められるのに対し，*chat-GluR2*-Tg 7 とのダブルトランスジェニックマウスでは，構造異常体形成が 2ヵ月近く遅れているのがわかる[9]．

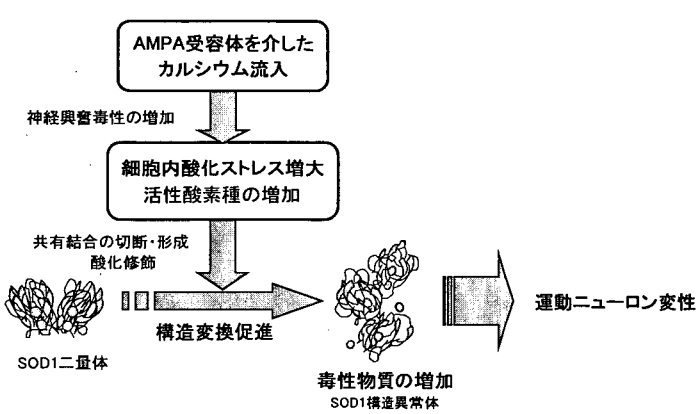

図 3　カルシウム透過型 AMPA 受容体を介した運動ニューロン変性(仮説)

脊髄運動ニューロンではグルタミン酸刺激によりカルシウム透過型 AMPA 受容体が活性化され，ミトコンドリアにおける活性酸素種の生成が促進される[12]．活性酸素種の増加により変異型 SOD 1 タンパクの構造変換が促進され，構造異常体の細胞毒性により運動ニューロン変性が引き起こされると考えられる．

体は運動ニューロン変性の促進因子であり，変異 SOD 1 の存在下では変異 SOD 1 タンパクの毒性を促進して ALS 発症を早める危険因子であることが示された．

カルシウム透過型 AMPA 受容体による SOD 1 構造異常体形成促進

次に我々は，カルシウム透過型 AMPA 受容体が変異 SOD 1 毒性を促進するメカニズムについて解析した．異常タンパク仮説を踏まえ，マウス脊髄の細胞分画を行い，毒性を有するとされる構造異常体の細胞内分布・出現時期に及ぼす影響を調べた(図 2)[9]．*hSOD1*^{G93A}-Tg では発症の 3ヵ月前(4ヵ月齢)には核およびミトコンドリア分画に SOD 1 構造異常体が検出され，発症期には他分画にも広がり，病気の進行とともに飛躍的に蓄積していく．これに対し *chat-GluR2*-Tg 7 とのダブルトランスジェニックマウスでは，構造異常体の出現パターンは変わらないが出現時期が 2ヵ月近く遅れていた．この結果は AMPA 受容体のカルシウム透過性が下がると SOD 1 構造異常体の形成が遅れることを示している．変異 SOD 1 タンパクの構造変換は酸化修飾によって著しく促進されるので[3,4]，脊髄抽出液中のタンパクの酸化修飾レベルを代表的な酸化修飾であるカルボニル化を指標に定量化した[9]．*hSOD1*^{G93A}-Tg では

構造異常体の出現と同調してカルボニル化されたタンパク量が上昇するが，Tg 7 とのダブルトランスジェニックマウスでは構造異常体の遅延と同様に約2ヵ月遅れていた．よってカルシウム透過型AMPA受容体の発現は運動ニューロン内における酸化修飾反応を促進し，その結果，変異SOD 1タンパクの構造変換が促進されている可能性が強く示唆された．培養下の脊髄運動ニューロンでは，グルタミン酸刺激後，AMPA受容体を介して流入したカルシウムが一過的にミトコンドリアに移行して，ミトコンドリアにおける活性酸素種の生成増大をもたらすことが報告されている[12]．これらの結果を総合すると，脊髄運動ニューロンではグルタミン酸に曝されるたびにカルシウム透過型AMPA受容体を介して細胞内酸化ストレスが上昇し，過剰に生成された活性酸素種が変異SOD 1タンパクの構造変換を促進する，という反応が繰り返されていることが予想される(図3)[13]．

▣ むすび

本稿では家族性ALSモデルマウスでの知見をもとに，脊髄運動ニューロンが特異的に発現しているAMPA受容体のサブタイプ(カルシウム透過型)が，細胞内酸化ストレスの上昇を介して原因遺伝子産物の毒性型への変換を促進している可能性を紹介した．紙面の都合上割愛したが，孤発性ALSにおいてもカルシウム透過型AMPA受容体の増加と発症との関係が注目されている[14]．GluR 2サブユニットはRNA編集による厳密な制御を受けており，この編集機構が破綻した場合にも受容体はカルシウム透過性となる．孤発性ALS患者の脊髄運動ニューロンではGluR 2の編集効率が有意に低下しており，よって家族性ALSにおける変異SOD 1タンパクと同様に，ある種のタンパクの酸化修飾・構造変換が亢進されて運動ニューロン変性が引き起こされている可能性が考えられる．したがって，この受容体サブタイプを特異的に阻害または減少させる手段が開発されれば，現在有効な治療法のないALS患者一般を救うことができるかもしれない．

文 献

1) Julien JP. Amyotrophic lateral sclerosis : unfolding the toxicity of the misfolded. Cell. 2001 ; 104 : 581-91.
2) Bruijn L, Miller TM, Cleveland DW. Unraveling the mechanisms involved in motor neuron degeneration in ALS. Annu Rev Neurosci. 2004 ; 27 : 723-49.
3) Valentine JS, Hart PJ. Misfolded CuZnSOD and amyotrophic lateral sclerosis. Proc Natl Acad Sci USA. 2003 ; 100 : 3617-22.
4) Urushitani M, Kurisu J, Tsukita K, et al. Proteasomal inhibition by misfolded mutant superoxide dismutase 1 induces selective motor neuron death in familial amyotrophic lateral sclerosis. J Neurochem. 2002 ; 83 : 1030-42.
5) Shibata N, Asayama K, Hirano A, et al. Immunohistochemical study on superoxide dismutases in spinal cords from autopsied patients with amyotrophic lateral sclerosis. Dev Neurosci. 1996 ; 18 : 492-8.
6) Watanabe M, Dykes-Hoberg M, Culotta VC, et al. Histological evidence of protein aggregation in mutant SOD 1 transgenic mice and in amyotrophic lateral sclerosis neural tissues. Neurobiol Dis. 2001 ; 8 : 933-41.
7) Shaw PJ, Eggett CJ. Molecular factors underlying selective vulnerability of motor neurons to neurodegeneration in amyotrophic lateral sclerosis. J Neurol. 2000 ; 247 Suppl 1 : I 17-27.
8) Maragakis NJ, Rothstein JD. Glutamate transporters : animal models to neurologic disease. Neurobiol Dis. 2004 ; 15 : 461-73.
9) Tateno M, Sadakata H, Tanaka M, et al. Calcium-permeable AMPA receptors promote misfolding of mutant SOD 1 protein and development of amyotrophic lateral sclerosis in a transgenic mouse model. Hum Mol Genet. 2004 ; 13 : 2183-96.
10) Kuner R, Groom AJ, Bresink I, et al. Late-onset motor neuron disease caused by a functionally modified AMPA receptor subunit. Proc Natl Acad Sci USA. 2005 ; 102 : 5826-31.
11) Van Damme P, Braeken D, Callewaert G, et al. GluR 2 deficiency accelerates motor neuron degeneration in a mouse model of amyotrophic lateral sclerosis. J Neuropathol Exp Neurol. 2005 ; 64 : 605-12.
12) Carriedo SG, Sensi SL, Yin HZ, et al. AMPA exposures induce mitochondrial $Ca^{(2+)}$overload and ROS generation in spinal motor neurons in vitro. J Neurosci. 2000 ; 20 : 240-50.
13) Rao SD, Weiss JH. Excitotoxic and oxidative cross-talk between motor neurons and glia in ALS pathogenesis. Trends Neurosci. 2004 ; 27 : 17-23.
14) Kwak S, Kawahara Y. Deficient RNA editing of GluR 2 and neuronal death in amyotrophic lateral sclerosis. J Mol Med. 2005 ; 83 : 110-20.

ARTICLE IN PRESS

BRAIN RESEARCH XX (2006) XXX–XXX

available at www.sciencedirect.com

SCIENCE DIRECT®

www.elsevier.com/locate/brainres

BRAIN RESEARCH

Short Communication

Localization of Id2 mRNA in the adult mouse brain

Kazuhito Kitajima[a,b,c], *Ryosuke Takahashi*[c], *Yoshifumi Yokota*[a,*]

[a]*Department of Molecular Genetics, School of Medicine, University of Fukui, 23-3 Shimoaizuki, Matsuoka, Fukui 910-1193, Japan*
[b]*Department of Neurology, Fukui Red Cross Hospital, 2-4-1 Tsukimi, Fukui 918-8501, Japan*
[c]*Department of Neurology, Graduate School of Medicine, Kyoto University, 54 Shogoin Kawahara-cho, Sakyo 606-8507, Kyoto, Japan*

ARTICLE INFO

Article history:
Accepted 12 December 2005

Keywords:
Helix–loop–helix protein
Id2
Gene expression
Adult brain
Mouse

Abbreviations:
bHLH, basic helix–loop–helix
HLH, helix–loop–helix
DEPC, diethylpyrocarbonate

ABSTRACT

Id proteins are negative regulators of basic helix–loop–helix transcription factors and are involved in cellular differentiation and proliferation. Four members of the Id gene family exhibit closely related but distinct expression patterns in various mammalian organs of not only embryos but also adults. Among them, Id2 is known to be expressed in Purkinje cells and neurons in the cortical layers of the adult mouse brain, suggesting that Id2 is involved in some neural functions in the adult. To get insight into the role of Id2 in the nervous system, we investigated the localization of Id2 mRNA-expressing cells in the adult mouse brain in detail by in situ hybridization with the radiolabeled antisense probe and compared it with the localization of other Id gene family members. The results indicated that Id2 mRNA is detected in more varied brain regions than previously reported. These regions include the amygdaloid complex, caudate putamen, globus pallidus, substantia nigra pars reticulata, suprachiasmatic nucleus, and the anterior part of the subventricular zone. These results suggest the possibility that Id2 plays a role in the neural activity and cognitive functions. On the other hand, Id1 was barely detectable. Although moderate or low expression of Id3 was observed diffusely, high expression was observed in some specific regions including the molecular layer of the dentate gyrus and the external capsule. Id4 mRNA was detected in the regions such as the caudate putamen and the lateral amygdaloid nucleus. Thus, the expression pattern of Id2 is distinct from those of other Id gene family members.

Transcription factors play essential roles in various biological processes including cellular differentiation and proliferation by regulating gene expression. They are categorized according to their structural similarities. The basic helix–loop–helix (bHLH) protein family is a typical example. The members of this family share structural characteristics of the basic region and the helix–loop–helix (HLH) domain, which are required for DNA binding and dimerization, respectively (Massari and Murre, 2000). In general, tissue-specific bHLH factors form heterodimers with ubiquitously expressed bHLH factors, so-called E proteins consisting of E2A gene products (E12 and E47), HEB and E2-2, and regulate the expression of their respective target genes via the consensus-binding site, the E box (Massari and Murre, 2000). Tissue-specific bHLH factors that exhibit a high degree of sequence conservation constitute subfamilies and are involved in similar biological processes (Kageyama and Nakanishi, 1997; Massari and Murre, 2000). For example, neurogenic bHLH factors, such as NeuroD and Mash1, play

Corresponding author. Fax: +81 776 61 8164.
E-mail address: yyokota@fmsrsa.fukui-med.ac.jp (Y. Yokota).

0006-8993/$ – see front matter © 2005 Elsevier B.V. All rights reserved.
doi:10.1016/j.brainres.2005.12.048

important roles in cell fate determination, specification and proliferation control during neurogenesis in a wide variety of species by constituting gene regulatory cascades and carrying out their specific functions (Kageyama and Nakanishi, 1997; Massari and Murre, 2000).

Id proteins, inhibitors of DNA binding/differentiation, are negative regulators of bHLH transcription factors, and four members of this protein family, Id1–Id4, have been identified in mammals (Massari and Murre, 2000; Ruzinova and Benezra, 2003). They possess HLH domains and form heterodimers with bHLH factors, but the resultant heterodimers are unable to bind DNA due to the lack of a DNA-binding domain in Id proteins (Massari and Murre, 2000; Ruzinova and Benezra, 2003). Thus, Id proteins inhibit the functions of bHLH factors in a dominant negative manner and suppress bHLH factor-dependent cellular differentiation (Massari and Murre, 2000; Ruzinova and Benezra, 2003). On the other hand, Id proteins have the ability to stimulate cell cycle progression. Although the mechanism remains unclear, Id proteins have been reported to have abilities to inhibit the enhanced expression of cyclin-dependent inhibitors such as p21 by bHLH factors and to antagonize the activity of Rb family proteins (Ruzinova and Benezra, 2003; Yokota and Mori, 2002). Based on these functional characteristics, Id proteins are thought to be involved in the regulation of cell differentiation and in the expansion of immature cell populations (Ruzinova and Benezra, 2003; Yokota and Mori, 2002). In fact, each member of the Id gene family is expressed in a wide range of embryonic tissues including the central nervous system, and different members show similar but distinct expression patterns (Andres-Barquin et al., 2000; Jen et al., 1996, 1997; Neuman et al., 1991; Rubenstein et al., 1999; Tzeng and de Vellis, 1998). Id genes are also expressed in the adult central nervous system (Andres-Barquin et al., 2000; Elliott et al., 2001; Neuman et al., 1991; Riechmann et al., 1994; Rubenstein et al., 1999; Tzeng and de Vellis, 1998), although there is a tendency for the expression levels to decrease (Andres-Barquin et al., 2000; Neuman et al., 1991; Tzeng and de Vellis, 1998). For example, Id2 is expressed in neurons in all layers of the cerebral cortex except layer 4, Purkinje cells of the cerebellum, the olfactory bulb (the mitral cell, glomerular and internal granule cell layers), the hippocampus, and the suprachiasmatic nucleus (SCN) of the adult rodent brain (Andres-Barquin et al., 2000; Elliott et al., 2001; Neuman et al., 1991; Rubenstein et al., 1999; Tzeng and de Vellis, 1998; Ueda et al., 2002). These observations suggest that Id proteins are involved in cellular functions in terminally differentiated and non-dividing cells, in addition to playing roles in cell differentiation and proliferation control.

To get insight into the role of Id2 in neural functions, we investigated the distribution of Id2 mRNA in the adult mouse brain by in situ hybridization. Adult male mice of ICR or the mixed genetic background between NMRI and 129/Sv were used in this study. Similar results were obtained from the two strains. Mice were deeply anesthetized with diethyl ether and perfused transcardially with PBS followed by fixative containing 4% paraformaldehyde in PBS. After perfusion, the brain was taken out of the skull, immersed in the same fixative for 24 h at 4 °C, transferred to 0.1% diethylpyrocarbonate (DEPC)-treated 20% sucrose in PBS for 48 h at 4 °C, and then frozen with OCT compound at −80 °C. The brain was cut into 10- m-thick sections on a cryostat and mounted on glass slides. Sections were stored at −80 °C until use. All animal procedures were performed in accordance with the guidelines of the University of Fukui for animal experiments. In situ hybridization was performed as described (Ishii et al., 1990; Mori et al., 2000). Briefly, 10- m-thick coronal sections were treated with 5 g/ml proteinase K and acetylated before hybridization. An ^{35}S-labeled RNA probe spanning nt 61–759 of the mouse Id2 cDNA was generated by transcription with RNA polymerase using the pBS-Id2 plasmid as template (Mori et al., 2000). The sections were hybridized in the presence of 50% formamide at 60 °C overnight, washed at high stringency, dipped with NTB2 emulsion (Kodak), and autoradiographed. The sections were then counterstained with the Cresyl Fast Violet solution to allow morphological identification. Anatomical determinations were made according to a standard atlas (Paxinos and Franklin, 2001). In situ hybridization of brain sections with the ^{35}S-labeled sense probe gave no appreciable signal and confirmed the specificity of the ^{35}S-labeled antisense probe for the detection of the Id2 mRNA (data not shown).

In the main olfactory bulb, Id2 mRNA was expressed in the mitral, glomerular, and granule cell layers (Mi, Gl, GrO) (Fig. 1A and Table 1), as reported (Neuman et al., 1991). In the anterior olfactory nucleus, both medial (AOM) and posterior (AOP) parts were stained (Fig. 1B). In the septum, Id2 mRNA was moderately expressed in the lateral septal nucleus, intermediate and ventral part (LSI and LSV, respectively) (Fig. 1C), although the expression level was lower in the lateral septal nucleus, dorsal part (LSD), and medial septal nucleus (MS) (Fig. 1C). Some Id2-expressing cells were distributed in the corpus callosum (cc) (Figs. 1C, 3E), in accordance with the report about Id2 mRNA expression in S100$^+$GFAP$^+$ astrocytes and GFAP$^-$ and O4$^-$ cells in the rat corpus callosum (Tzeng and de Vellis, 1998).

In the cerebral cortex, Id2 mRNA was detected in all layers except layer 4, and scattered cells were positive for Id2 mRNA in layer 1 (Figs. 1B–G, 2A–C). Strong Id2 mRNA expression was observed in layer 5 of the neocortex as reported (Figs. 1C–F) and in layer 2 in the piriform cortex (Pir) (Figs. 1B–D). In the cingulate (Cg/RS) and retrosplenial cortices (RS), the level of Id2 mRNA expression was high in layers 2 and 3 (Figs. 1E and F).

Strong expression of Id2 mRNA was observed in the many regions of the amygdaloid complex: the basolateral amygdaloid nucleus anterior part (BLA), lateral amygdaloid nucleus dorsolateral part (LaDL), ventromedial part (LaVM), ventrolateral part (LaVL), medial amygdaloid nucleus posterodorsal part (MePD), posteroventral part (MePV), posteromedial cortical amygdaloid nucleus (PMCo), and intercalated nuclei of the amygdala (I) (Figs. 1D–G and 3A). In the other subnuclei, moderately expressing cells were distributed (Fig. 3A). In addition, moderate expression was observed in the dorsal and ventral parts of the anterior amygdaloid area (AAD, AAV), anterior cortical amygdaloid nucleus (ACo), and nucleus of the lateral olfactory tract (LOT) (Fig 1D). High expression was also seen in the dorsal endopiriform nucleus (DEn) (Figs. 1B and F, 3A). Moderate expression was also observed in the bed nucleus of stria terminalis (BST) (Fig. 1D) and the intraamygdaloid division of the bed nucleus of the stria terminalis